

**Recent advances in electrochemiluminescence**

Journal:	<i>Chemical Society Reviews</i>
Manuscript ID:	CS-REV-01-2015-000086.R1
Article Type:	Review Article
Date Submitted by the Author:	06-Mar-2015
Complete List of Authors:	Liu, Zhongyuan; Changchun Institute of Applied Chemistry, The State Key Laboratory of Electroanalytical Chemistry Qi, Wenjing; Changchun Institute of Applied Chemistry, The State Key Laboratory of Electroanalytical Chemistry Xu, Guobao; Chanchun Institute of Applied Chemistry,

Cite this: DOI: 10.1039/c0xx00000x

www.rsc.org/xxxxxx

ARTICLE TYPE

Recent advances in electrochemiluminescence

Zhongyuan Liu^{†a}, Wenjing Qi^{†a, b} and Guobao Xu^{*a}

Received (in XXX, XXX) Xth XXXXXXXXX 20XX, Accepted Xth XXXXXXXXX 20XX

DOI: 10.1039/b000000x

The great success of electrochemiluminescence (ECL) for *in vitro* diagnosis (IVD) and the promising potential in light-emitting devices greatly promotes recent ECL study. More than 45% of ECL articles were published after 2010, and the first international meeting on ECL was held in Italy in 2014. This critical review discusses recent vibrant developments in ECL, and highlights novel ECL phenomena, such as wireless ECL devices, bipolar electrode-based ECL, light-emitting electrochemical swimmers, upconversion ECL, ECL resonance energy transfer, thermoresponsive ECL, ECL using shape-controlled nanocrystals, ECL as ion-selective electrode photonic reporter, paper-based microchip, and self-powered microfluidic ECL platform. We also comment the latest progress in bioassays, light-emitting devices and, computational approach for ECL mechanism study. Finally, perspectives and key challenges in near future are addressed (198 references).

1. Introduction

Electrochemiluminescence (ECL) is an electrogenerated chemiluminescence (CL) phenomenon with hundreds of millions dollars in sales per year.¹⁻⁴ It has been extensively studying recently, particularly on bioanalysis, nanomaterials and light-emitting devices. Most recent studies mainly utilize metal complexes, luminol, and nanomaterials as ECL luminophores. The extensive studies of ECL of metal complexes are attributed to three main reasons. First, tris(2,2'-bipyridine)ruthenium(II) ($\text{Ru}(\text{bpy})_3^{2+}$) ECL has achieved the overwhelming success for *in vitro* diagnosis (IVD) because of its extremely high sensitivity, wide dynamic range, rapidness, simplicity, and stable labels by coupling with immunoassays and DNA probe assays. Second, metal complex ECL, particularly ruthenium complex ECL, allows the direct detection of numerous coreactants, leading to extremely broad applications. Third, metal complexes, particularly iridium complexes, enable easy color tuning for light-emitting devices and analytical applications. The popularity of luminol mainly results from its low cost, easy functionalization, and broad bioanalytical applications. In comparison with molecular luminophores, nanoluminophores, such as nanocrystals, metal nanoclusters, carbon nanomaterials, have been discovered recently. The versatility and expected fine properties of nanoluminophores arouse much research interests.

A literature survey using Web of Science shows that about 4700 ECL journal articles have been published since the first detailed ECL studies by Hercules and Bard et al. in the mid-1960s. More than 45% of ECL articles were published after 2010 (fig. 1). More excitingly and encouragingly, the first international meeting on electrogenerated chemiluminescence (ECL 2014) was held fifty years after the first detailed ECL studies. Accompanying with the rapid development of ECL, some excellent ECL reviews on nanomaterials and biosensors

appeared.⁵⁻¹³ Most reviews either were published some years ago or only focused on one particular aspect of ECL. Thus, this review will highlight significant developments since 2010, such as new systems, novel strategies, intriguing phenomena, recent applications, wireless devices, and computational approach for ECL mechanism study.

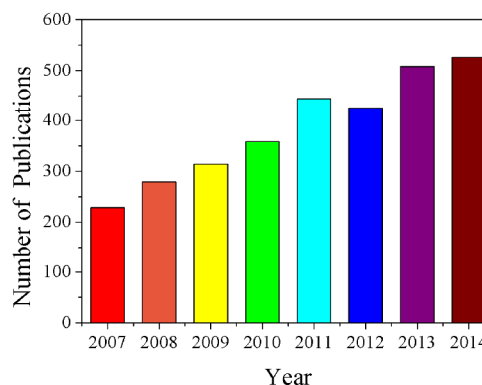


Fig. 1 ECL journal publication numbers as a function of year according to Thomson ISI Web of Science. Please see Ref. 1 for publication numbers before 2007.

2. Main ECL systems

2.1 Inorganic systems

2.1.1 Ruthenium complexes

$\text{Ru}(\text{bpy})_3^{2+}$ is the first inorganic complex ECL luminophore and is the most successful luminophore with very broad applications. The great achievement of $\text{Ru}(\text{bpy})_3^{2+}$ ECL as well as excellent chemical, electrochemical, and ECL properties of ruthenium complexes lead to the extensive study of new ruthenium complex

ECL systems to improve color tunability, light-emitting efficiency, applicability, and so on.

Most of ruthenium complexes have a maximum wavelength between 600 and 650 nm. It is difficult to tune the color of ruthenium complexes owing to the limited ligand-field splitting energies of central metal ions of ruthenium complexes. Inspiringly, a new series of acrylate-containing Ru(bpy)₃²⁺ complexes (compounds **1-4**, fig. 2) with photoluminescence emission maxima ranging from 640 to 700 nm have been reported.¹⁴ The large red shift in the photoluminescence emission (fig. 3) probably arises from a decrease in their ligand-based lowest unoccupied molecular orbital (LUMO) value and the resulting lower energy triplet metal-to-ligand charge-transfer excited state transitions. The ECL emission maxima of these compounds are in the range of 688 to 722 nm. It is the lowest-energy emission reported so far in light-emitting electrochemical cells (LECs) based on tris-chelated ruthenium complexes. Moreover, the polymer films of these compounds show polyelectrochromic behaviours and are appealing materials for electrochromic devices.

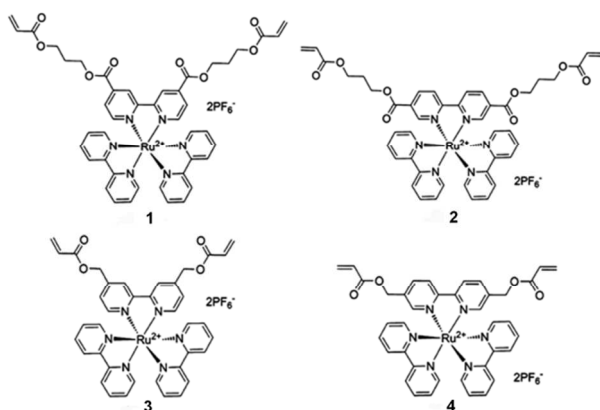


Fig. 2 Acrylate-containing Ru(bpy)₃²⁺-based coordination complexes reported in ref. 14. Reprinted with permission from ref. 14.

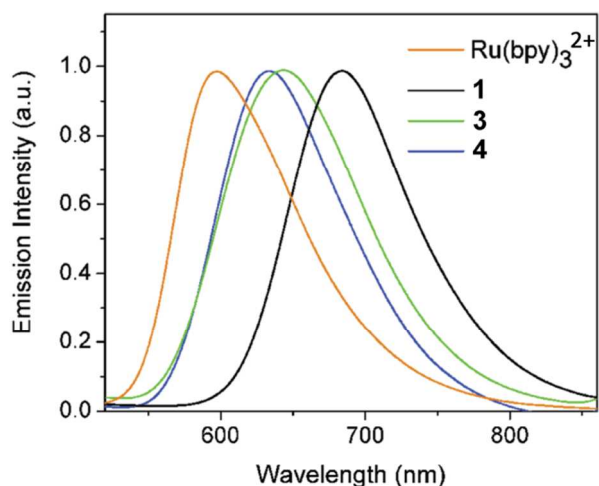


Fig. 3 Normalized photoluminescence spectra obtained from thin solid films of compounds **1**, **3**, **4**, and Ru(bpy)₃²⁺ with excitation wavelength at 450 nm. Reprinted with permission from ref. 14.

In comparison with annihilation ECL widely used in LECs,

coreactant ECL of ruthenium complexes plays much more important roles in analytical applications. Coreactant ECL of ruthenium complexes involves the reactions between ruthenium complexes and coreactants. The ECL efficiencies of coreactant ECL not only are dependent on the photoluminescence quantum yields, but also are sensitive to minor change in the structures of ruthenium complexes. Thus the investigation of the structure effects of ruthenium complexes has received much attention. The ECL properties of Ru(II) heteroleptic complexes ([Ru(BPS)_n(bpy)_{3-n}]⁽²ⁿ⁻²⁾⁻ bearing mixed 2,2'-bipyridine (bpy) and bathophenanthrolinedisulfonate (BPS) ligands were examined, where as *n* decreases from 3 to 1, the net charge changes from -4 to 0.¹⁵ Surprisingly, ECL intensities increased approximately 5 to 26 times with respect to Ru(bpy)₃²⁺ as *n* decreased from 3 to 1 by using tripropylamine (TPA) as coreactant and applying a constant potential. The increase in ECL intensities of [Ru(BPS)_n(bpy)_{3-n}]⁽²ⁿ⁻²⁾⁻ with decreasing *n* was correlated with the complex net charge. The highly negative charge promoted the formation of filming products at the electrode during oxidation, resulting in the reduced ECL intensity. The formation of filming products was suppressed when the negative charge was reduced or eliminated, resulting in the enhanced ECL intensity. It is apparent from this study that reducing or eliminating the complex negative charge for enhanced ECL is possible.

Coreactant ECLs mainly include oxidative-reductive ECL and reductive-oxidative ECL.^{16, 17} Oxidative-reductive ECLs generally occur at positive potentials where oxygen evolution is very slow in aqueous solutions and has little effect on ECL. It is thus easy to realize oxidative-reductive ECL. In contrast, many reductive-oxidative ECL systems require very negative potentials where hydrogen evolves vigorously and electrogenerated intermediates decompose immediately, making it challenging to achieve stable reductive-oxidative ECL in aqueous solutions. A tricresyl phosphate-based carbon paste electrode was introduced to address the problem.¹⁶ It exhibited extremely high hydrogen evolution potential (lower than -1.6 V) and could dramatically stabilize electrogenerated intermediate Ru(bpy)₃⁺ that is highly unstable in aqueous solutions (fig. 4). As a result, reversible Ru(bpy)₃^{2+/1+} wave has been achieved in aqueous solutions for the first time at a low scan rates, and strong cathodic ECL of Ru(bpy)₃^{2+/S₂O₈²⁻} in aqueous solutions were observed. It suggests that carbon paste electrodes with suitable pasting liquids provide versatile platforms for electrochemical study at very negative potentials.

Besides luminophores, ECL coreactants have also received much attention since coreactant pathway plays a dominant role in current ECL field.¹⁷ TPA is an efficient coreactant widely used in commercial assays. However, the electro-oxidation of TPA itself can produce a weak ECL background signal even in the absence of luminophores, such as Ru(bpy)₃²⁺, limiting the sensitivity of ECL analytical methods.¹⁸ The nature of this reaction is not understood very clearly for many years, e.g., what species in this system is the ultimate ECL emitter and how it is produced. Recently, a very interesting research¹⁹ has demonstrated that background ECL emission at 630 nm observed during the electrochemical oxidation of TPA in the presence of dissolved O₂ in acetonitrile solution can be attributed to the dimeric ¹Δ_g state of

O₂. The formation of the excited state is based on the reaction between dissolved oxygen and two different products of TPA oxidation: the TPA• radical that reduces O₂ to the superoxide ion and the TPA^{•+} radical cation that oxidizes this species to singlet O₂. No ECL emission was observed when the same solution in the absence of dissolved O₂. These results suggest that the sensitivity of analytical applications of ECL could be improved by the rigorous exclusion of O₂.

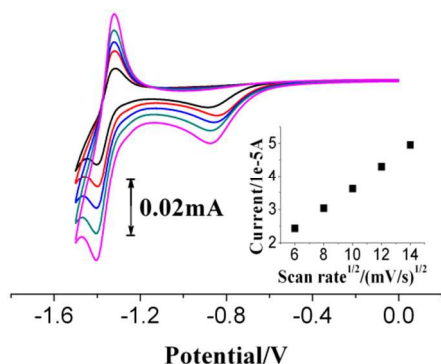


Fig. 4 The influence of scan rate on cyclic voltammograms at the tricresyl phosphate-based carbon paste electrode in 0.1 M phosphate buffer solution (pH 7.5) containing 1 mM Ru(bpy)₃²⁺. Scan rate, 36, 64, 100, 144, and 196 mV s⁻¹. Reprinted with permission from ref. 16.

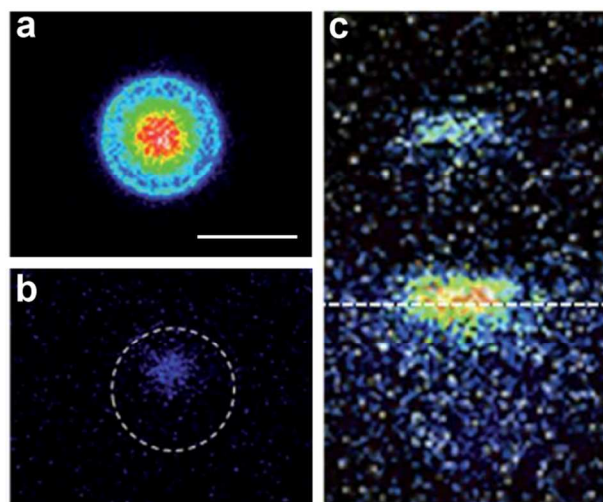


Fig. 5 (a and b) Top-view ECL images of 12 μm ruthenium label functionalized polystyrene beads. The ECL images were measured in phosphate buffer solutions containing (a) 100 mM TPA or (b) 20 mM DBAE on glassy carbon electrodes. The dashed line displays the position of the bead. (c) Side-view ECL images of a 12 μm ruthenium complex labelled polystyrene bead in a phosphate buffer solution containing 100 mM TPA (pH 7.4) on glassy carbon electrode. The dashed line displays the position of the glassy carbon electrode surface (i.e. z = 0). Scale bar: 10 μm. Reprinted with permission from ref. 21.

TPA and 2.8 μm diameter magnetic beads with Ru(bpy)₃²⁺-tagged species are employed in the commercial Origen analyzer. Scanning ECL microscopy study suggests that intermediates generated by the electrooxidation of TPA can move up to 5~6 μm to cause the excitation of Ru(bpy)₃²⁺, resulting in the high sensitivity of ECL assays.²⁰ In comparison with TPA, user-friendly 2-(dibutylamino)ethanol (DBAE) exhibits much higher efficiencies at gold electrodes and platinum electrodes in the

presence of low concentrations of Ru(bpy)₃²⁺ in solutions. To better understand the extremely high sensitivity of the Ru(bpy)₃²⁺/TPA system and the Ru(bpy)₃²⁺/DBAE system, a 3D imaging technique was utilized to provide a global description of the ECL reactivity at the single Ru(bpy)₃²⁺-functionalized bead level.²¹ As shown in fig. 5, ECL emerges from the entire 12 μm bead with a brighter spot in bead center for the Ru(bpy)₃²⁺/TPA system and weaker ECL was observed in the bead center over a ~4-5 μm diameter surface for the Ru(bpy)₃²⁺/DBAE system. The different ECL performance of TPA and DBAE with freely diffusing Ru(bpy)₃²⁺ in solutions and Ru(bpy)₃²⁺ attached to microbeads indicates that the DBAE-derived radicals were less stable than the TPA ones and the stability of intermediates play very important role for sensitive detection in bead-based bioassays. Side-view image shows a brighter region at the top of 12 μm bead for the Ru(bpy)₃²⁺/TPA system, indicating that the bead can act as a lens to focus ECL emission for improving sensitivity. The 3D imaging technique provides a new way for ECL mechanistic study and new strategy to select new coreactants. For example, coreactants generating relatively stable intermediates may benefit for bead-based bioassays and coreactants generating relatively active intermediates may benefit for bead-free bioassays and homogeneous bioassays to improve selectivity.

To extend ECL applications and improve ECL efficiencies, many efforts have also been made to find new coreactants for Ru(bpy)₃²⁺ ECL.²²⁻²⁴ It was reported that glyoxal, methylglyoxal, and glyoxylic acid exhibited better ECL efficiency than the well-known coreactant oxalate at glassy carbon electrode.²⁵ Mechanism studies indicate that electrogenerated hydroxyl radicals play important roles in ECL, implying that coreactant family can be expanded by taking advantage of the strong oxidation ability of electrogenerated hydroxyl radicals at boron doped diamond electrodes. Surprisingly, ozone can highly effectively quench ECL of Ru(phen)₃²⁺/glyoxal.²⁶ It can almost quench ECL totally even at an ozone/glyoxal ratio of less than 0.5% (fig. 6). The remarkable ECL quenching efficiencies are ascribed to the formation of polyglyoxals by condensation reactions and the deactivation of polyglyoxals by ozone since both the quenching of excited Ru(phen)₃²⁺ and the oxidation of glyoxal to form carbon dioxide are negligible at low ozone concentrations. This study shows a new strategy for developing highly effective quenching system and sensitive detection method through the chain quenching reaction of polymers and nanomaterials.

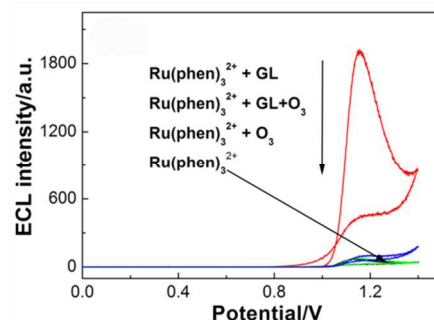


Fig. 6 Comparison of the ECL-potential curves of Ru(phen)₃²⁺ (black curve) in the presence of ozone (green curve), glyoxal (GL, red curve), and glyoxal and

ozone (blue curve) at the glassy carbon electrode. $c(\text{Ru}(\text{phen})_3^{2+})$, 0.5 mM; $c(\text{ozone})$, 20 μM ; $c(\text{glyoxal})$, 5 mM; scan rate: 0.1 V s^{-1} ; photomultiplier tube voltage, 1000 V. Reprinted with permission from ref. 26.

2.1.2 Iridium complexes

Iridium complexes are highly promising candidates with high quantum efficiencies for color tuning over ruthenium complexes due to higher ligand-field splitting energies of the trivalent iridium ion. Recently, charged complexes containing the cyclometalated Ir(III) moiety have been found to be more versatile in terms of color tunability and device efficiency. Iridium complexes have received increasing attention in ECL recently. With the development of LECs, a lot of cationic iridium complexes with emission in the yellow–orange region have been successfully developed. Currently, a great challenge is the development of blue-emitting complexes. Very recently, a number of blue-emitting iridium(III) complexes were explored.²⁷ Among these complexes, $[\text{Ir}(\text{df-ppy})_2(\text{ptb})]^+$ (**5**, fig. 7) was most potential as a blue-emitter for ECL detection, because it presented a considerable hypsochromic shift (ca. 60 nm) and over 16-fold greater coreactant ECL intensities than the parent $[\text{Ir}(\text{ppy})_3]$ complex, good solubility in polar solvents, and convenient synthesis of functionalized analogues that would be suitable for immobilization or ECL-labelling experiments. Meantime, the theoretical and experimental data together show that efficient blue-shifted ECL emission can be accomplished by stabilizing the highest occupied molecular orbital (HOMO) via anchoring electron-withdrawing substituents on the cyclometalated ligands, while only moderately stabilizing (or destabilizing) the LUMO via introducing electron-donating substituents on the neutral ancillary ligands, which will enlarge the HOMO–LUMO energy gap but ensure favourable thermodynamics and kinetics for the ECL reaction. According to this approach, fluorine substituents are commonly introduced as electron-withdrawing substituents into the cyclometalated ligand for blue-shift of the emission,^{28, 29} but the stabilities of the emitters in operating devices are usually decreased. To overcome this shortage, fluorine-free blue-green emitters using methoxy- and methyl-substituted 2,3'-bipyridine as the cyclometalated ligands (e.g. **6** in fig. 7) were presented.³⁰ The new complexes exhibit blue-green emission with maxima around 450 nm. In order to enlarge the energy gap, iridium complex **7** with phenylpyrazole as cyclometalated ligand instead of phenylpyridine (fig. 7) was developed.³¹ The developed complex not only exhibited enlarged energy gaps and blue-shifted emission spectrum as expected, but also showed improved device lifetime and color purity. Iridium complexes using aryltriazole as cyclometalated ligand instead of phenylpyridine (**8**, fig. 7) were also reported, and blue-shift emissions were obtained.³²

Green-emitting complexes and red-emitting complexes are also lacking.³³ To obtain green-emitting iridium complexes, a methylsulfone electron-withdrawing substituent (**9**, fig. 8) was introduced into the cyclometalated phenylpyrazole ligand to stabilize the HOMO.³⁴ Compared to complexes with the unsubstituted phenylpyridine ligand, the electron-withdrawing methylsulfone group led to a blue-shifted emission. Green electroluminescence is obtained by using these complexes in LECs. Two red-emitting iridium complexes **10** and **11** (fig. 8) with electroluminescence emission maxima ranging from 616 to 624 nm in LECs had been reported by using 1,3,4-oxadiazole

derivatives as the ancillary ligand and phenylpyridine as cyclometalated ligands.³⁵ By using 1,3,4-oxadiazole derivatives as both the cyclometalated ligands and the ancillary ligand, yellow-emitting iridium complexes with electroluminescence emission maxima ranging from 552 to 564 nm in LECs were attained. This provided a new way for tuning the light emission color of iridium compounds.

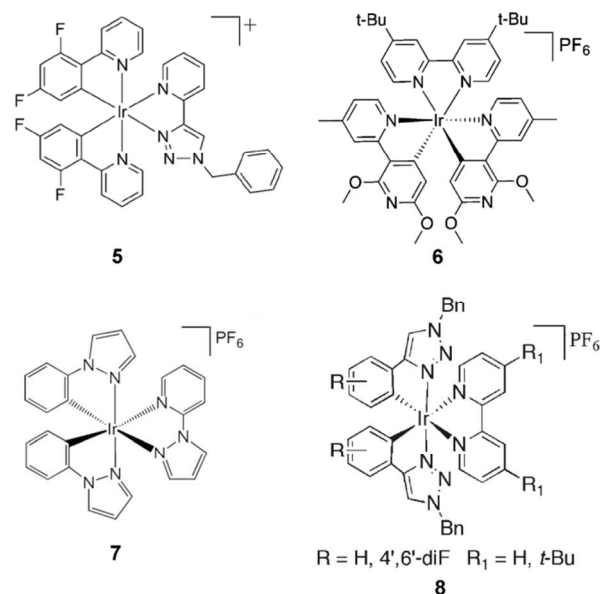


Fig. 7 Structure of Iridium(III) complexes **5–8**. **5**: Reprinted with permission from ref. 27. **6**: Reprinted with permission from ref. 30. **7**: Reprinted with permission from ref. 31. **8**: Reprinted with permission from ref. 32.

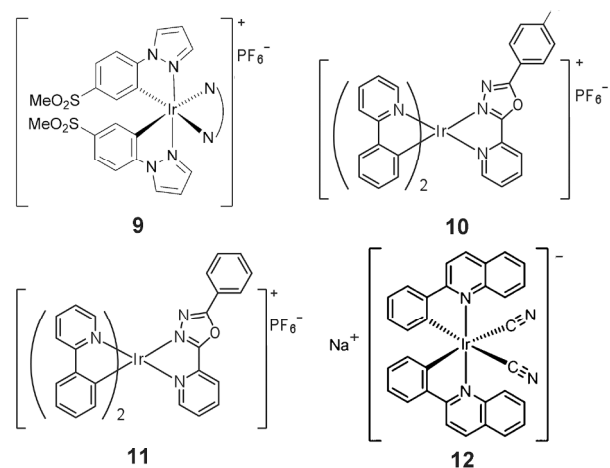


Fig. 8 Structural formula of Iridium(III) complexes **9–12**. **9**: Reprinted with permission from ref. 34. **10–11**: Reprinted with permission from ref. 35. **12**: Reprinted with permission from ref. 37.

Another challenge is to design ionic iridium complexes with UV emission. A series of charged iridium complexes emitting from UV to red have been recently reported based on pyridine-carbene (N^+C^-) as neutral ancillary ligand.³⁶ Owing to the very high LUMO of the carbene (N^+C^-) ligand, the emission derived from the main cyclometalated ligand, which is different from the commonly designed charged complexes with bidentate N^+N ancillary ligands, where the emission derived from the ancillary N^+N ligand. Attributed to intraligand ($\pi-\pi^*$) transitions, strong

bands in the UV up to 300 nm for these complexes were displayed in the UV-visible absorption spectra.

ECLs based on various cationic iridium complexes have been extensively reported with light emission wavelengths ranged from visible spectrum to near-UV. In contrast, ECLs using anionic iridium complexes are rarely reported. In 2012, Chen et al. reported two anionic iridium complexes and utilized them in LECs.³⁷ By adding 18-crown-6 to improve the film quality, LEC based on complex **12** (fig. 8) with high brightness and efficiency was achieved.

In addition to changing the ligand structure,^{38, 39} the emission colors of ECL systems can also be tuned by changing coreactant molecule,⁴⁰ pH of the solution,⁴¹ and frequency of applied current,⁴² or energy transfer processes.⁴³ Recently, a new strategy for color tunable ECL was developed through adjusting potential to tune the color of the ECL emission from a binary mixture of red light-emitting luminophore $[\text{Ru}(\text{bpy})_2(\text{L})]^{2+}$ and green light-emitting luminophore $[\text{Ir}(\text{df-ppy})_2(\text{BPS})]^-$.⁴⁴ A red-emitting $[\text{Ru}(\text{bpy})_2(\text{L})]^{2+}$ complex was selectively excited in the presence of a green-emitting $[\text{Ir}(\text{df-ppy})_2(\text{BPS})]^-$ at a moderate electrode potential (1.05 V vs. $\text{Fc}^{0/+}$), while simultaneous ECL from the two complexes was observed at high potentials (1.30 V vs. $\text{Fc}^{0/+}$), allowing the overall emission color to be tuned from red to yellow-green.^{44, 45} This approach opens new avenues for multianalyte ECL detection, and creates new possibilities for color selection in light-emitting devices. Whereafter, a potential-controlled switch on/off mechanism for selective excitation in mixed ECL systems was demonstrated by the same research group, which has important implications for potential-controlled ECL assays as it enables the selective excitation of luminophores on the basis of applied potential.⁴⁵

Potential control method was also used to tune the color of a three-color ECL system including a deep red emitter $[\text{Ru}(\text{bpy})_2(\text{dm-bpydc})]^{2+}$, a strong green emitter $\text{Ir}(\text{ppy})_3$, and a blue emitter $\text{Ir}(\text{df-ppy})_3$. By using a conventional camera as photo detector, a new strategy for color tunable ECL detection was also created.⁴⁶ The strategy exploited the distinct potentials required for the three above mentioned emitters' electrochemical excitation in conjunction with the inherent color selectivity of a conventional digital camera. The red, green, and blue ECL emitters in the same solution can be effectively resolved by modulating the applied potential used for excitation while simultaneously monitoring different emission wavelengths or color channels (fig. 9). Because the relative contribution ratio of each emitter to the photographic red-green-blue channels is constant, the red-green-blue ECL intensity versus applied-potential curves could be effectively isolated to a single emitter at each potential. The proposed potential-controlled color tunable ECL strategy is suitable for the development of low-cost, portable clinical diagnostic devices.

To promote the applications of more ECL labels in bioanalysis, which usually require at least some degree of water solubility, more water-soluble ECL labels are desired. But most iridium(III) complexes have low solubility in aqueous solution. To improve the water solubility, disulfonated bathophenanthroline ligands were incorporated to biscyclometalated iridium(III) complexes.⁴⁷ By this way, water-soluble biscyclometalated iridium(III) complexes were prepared, but the ECL intensities of these

complexes were lower than that of $\text{Ru}(\text{bpy})_3^{2+}$ reference. Owing to the good solubility, carbohydrates are usually introduced as functional groups to improve the solubility of substances.^{48, 49} Thus, water-soluble iridium(III) diimine complex with appended sugar was prepared, and the ECL behavior in aqueous buffer was also studied.⁵⁰ The ECL signal of this new iridium complex was much higher than that of $\text{Ru}(\text{bpy})_3^{2+}$ at a Pt working electrode. It has been applied to determine TPA and antibiotics with good sensitivity and reproducibility in aqueous buffer at Pt electrode. These complexes were promising alternatives to traditional tris-diimine ruthenium(II) complexes for ECL detection in aqueous phase, and provided convenient control of redox and luminescence properties using a variety of readily available ligands.

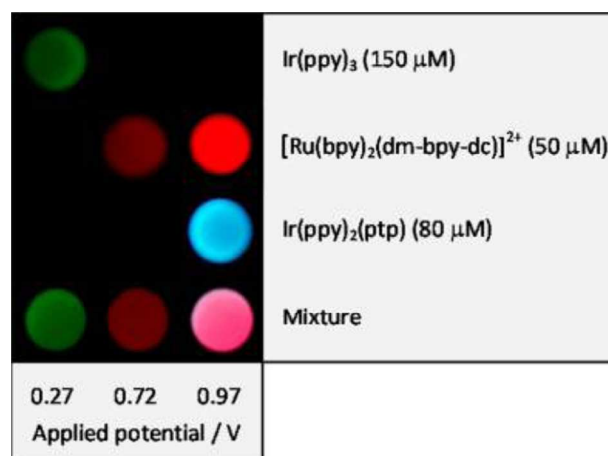


Fig. 9 Pictures of the ECL at the glassy carbon electrode surface at different applied potentials. Reprinted with permission from ref. 46.

2.2 Organic systems

Among the large number of organic emitters studied in ECL, 9,10-diphenylanthracene and its derivatives attracted increasing attention due to their remarkable luminescence properties in organic media.⁵¹⁻⁵³ 2- and 4-fold anthracene-functionalized tetraarylbimesityls **13-16** was synthesized and investigated (fig. 10).⁵¹ 2-fold anthracene-functionalized tetraarylbimesityls **13** and **14** exhibits two reversible, closely spaced one-electron transfers for both oxidation and reduction and 4-fold anthracene-functionalized tetraarylbimesityls **15** and **16** exhibits four reversible, closely spaced one-electron transfers for oxidation and reduction. The four compounds exhibited very strong ECL with emission at 480 nm, so that it can be seen with the naked eye.

To extend the applications in aqueous solutions, two hydrophilic diarylanthracenes, 9,10-bis(N-methylimidazolium-3-propoxyphenyl)anthracene (**DAA1**) and 9,10-bis(N-methylimidazolium-3-propoxy-2,6-dimethylphenyl) anthracene (**DAA2**) (fig. 11), were synthesized recently.⁵² Both **DAA1** and **DAA2** were soluble in aqueous medium and exhibited optical and electrochemical properties similar to that of the parent blue emitter 9,10-diphenylanthracene. Due to the steric hindrance caused by the dimethylphenyl substitution in **DAA2**, the active sites of the anthracene core were protected, avoiding undesired electrochemical reactions. Consequently, stable ECL emission of **DAA2** was observed in aqueous media. Since most organic emitters usually generate ECL in benzene/acetonitrile organic

solvent, it is of great importance that stable ECL emission of **DAA2** was observed even in aqueous media which is useful for its application in ECL bioanalysis combined with coreactant mediated oxidation. An alternative versatile strategy for improving the solubility in water and tuning the color of ECL is to dope ECL dyes in silica nanoparticles.⁴³ By using ECL-active dye 9,10-diphenylanthracene as the energy donor doped in the outer shell of the silica nanoparticles and fluorescent dye Rhodamine B derivative as the energy acceptor inserted into the silica core, the ECL emission were realized via an electrochemically induced energy transfer process between 9,10-diphenylanthracene doped in the outer shell and Rhodamine B derivative in the core of the nanoparticles. By using other suitable dye or two dyes in a cascade as the energy acceptor, the final colors of the ECL emission could be tuned and controlled. It is highly desirable that the development of innovative ECL multiple luminophores could increase the available colors and allow multiplexing ECL analysis.

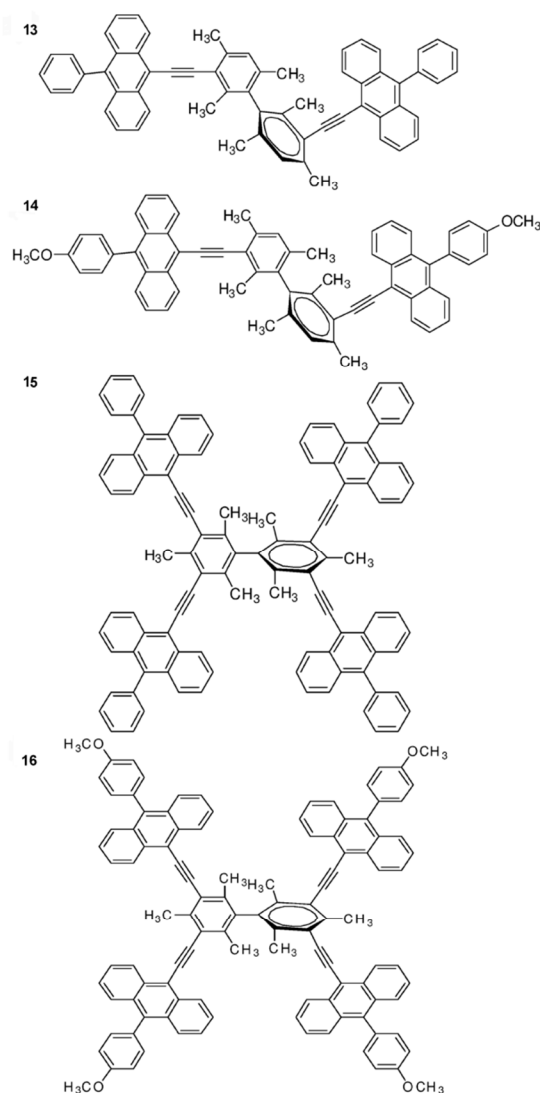


Fig. 10 Molecular structure of the 2- and 4-fold anthracene-functionalized bimesityl compounds: **13**, **14**, **15**, and **16**. Reprinted with permission from ref. 51.

In addition to anthracenes, fluorenes and derivatives are another class of important organic luminophores. The ECL of six π -stacked poly-(fluorenemethylene) oligomers (Fn, n = 1–6) by interactions between aromatic rings via π -stacking by van der Waals forces were investigated.⁵⁴ All six compounds gave a multiple, interacting one-electron transfer oxidation. The potentials for oxidation of the successive 1e transfers were explained in terms of electrostatic interactions among the fluorenes. As the number of fluorene units increased, the addition of the first electron to a fluorene oligomer became easier, and the stability of the radical cations also increased. No characteristic annihilation ECL signal was observed for them because of the extreme negative reduction potentials of these compounds, while a long-wavelength ECL emission at 550 nm of F6 was observed in the presence of coreactant C₂O₄²⁻.

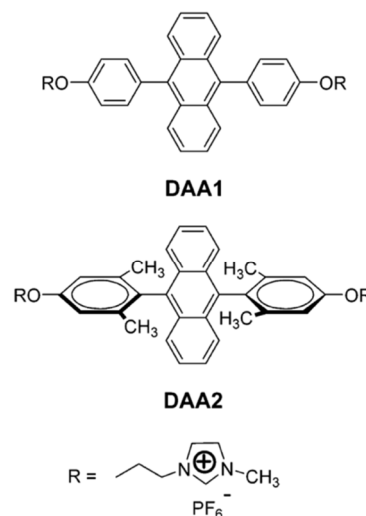


Fig. 11 Structure of aqueous soluble 9,10-Diarylanthracenes **DAA1** and **DAA2**. Reprinted with permission from ref. 52.

Due to the intrinsic tendency of aggregation of polyfluorenes, the emission wavelengths of LECs using polyfluorenes and derivatives as emissive materials are usually shifted to the green region. In order to avoid the aggregation for attaining blue-emitting LECs, low-molecular-weight analogues of polyfluorenes were designed. By covalent attachment of 1-methylimidazolium moieties to terfluorene as pendant groups, an ionic terfluorene derivative exhibiting a deep-blue emission with extremely high quantum yield was synthesized.⁵⁵ The successful strategy for achieving blue-emitting complexes promoted the further research on the molecules with larger energy gaps for attaining potential UV excitation light source for LECs. By covalent tethering of methylimidazolium moieties to 2,2'-bifluorene as pendant groups, an ionic 2,2'-bifluorene derivative with unprecedented UV emission was achieved, and the first UV LEC based on the ionic 2,20-bifluorene derivative was successfully realized, which exhibited UV electroluminescent emissions at ca. 386 nm.⁵⁶ The two above mentioned successful examples demonstrated that the molecular design strategy for ionic emitters is very suitable for LEC application.

Different from anthracenes and fluorenes, thienyltriazoles are C-N heterocyclic organic ECL compounds. Recently, four thienyltriazoles **17–20** (fig. 12) were synthesized via click

chemistry.⁵⁷ All the compounds were blue luminescent. They underwent irreversible redox reactions to generate electrochemically unstable radical anions and cations. Weak ECL from annihilation of these thienyltriazole radicals were observed in acetonitrile containing 0.1 M tetra-butylammonium perchlorate as electrolyte. Upon addition of benzoyl peroxide as the coreactant in acetonitrile, ECL efficiencies were enhanced ranging from 0.16 to 0.50 %. ECL intensities were enhanced about 90 times for **17**, 20 times for **18**, 100 times for **19**, and 10 times for **20**, bearing efficiencies of 0.50% for **17**, 0.16% for **18**, 0.35% for **19**, and 0.40% for **20**, relative to 9,10-diphenylanthracene in the coreactant system. A red-shift was observed for all four compounds in the ECL spectra relative to the corresponding photoluminescence spectra. This work is of importance for the development of efficient blue-emitting fluorophores via click chemistry.

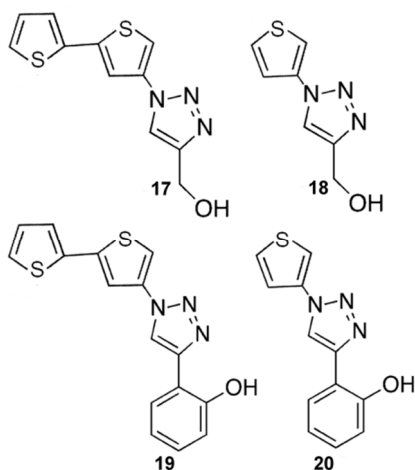


Fig. 12 Molecular structure of thienyltriazoles **17–20**. Reprinted with permission from ref. 57.

As another classic organic luminophore, luminol has been widely studied and continues to generate interest. Luminol ECL has two main categories, cathodic luminol ECL and anodic luminol ECL. The generation of cathodic luminol ECL often involves the electrochemical reduction of dissolved oxygen to generate reactive oxygen species (ROS). Cathodic luminol ECL usually is very weak since luminol is not oxidized on electrode at negative potentials. Anodic luminol ECL is generally weak in the absence of hydrogen peroxide due to difficult oxidation of water to generate ROS, and requires the addition of hydrogen peroxide.^{1,58} Recently, a new method to trigger luminol ECL with the addition of H₂O₂ was designed by electrochemical reduction followed by electrochemical oxidation using simple linear sweep voltammetry. By using this method, ROS is *in situ* generated by the electrochemical reduction of dissolved oxygen at negative potentials, and then luminol and electrogenerated ROS are oxidized as potentials are swept to positive potentials, resulting in about 500 times increase in ECL intensities.⁵⁹ This method is promising for other ROS-relevant ECL systems.

Due to the potential applications in modern light-emitting devices, donor-acceptor luminophores have attracted great interest. They are ECL emitters containing both donor and acceptor moieties in one molecule, which allow the generation of ECL by the annihilation reaction between the donor radical

cations and the acceptor radical anions without the addition of coreactant. Recently, four kinds of electron donor-acceptor molecules **21–24** (fig. 13) with high ECL efficiency of 50% have been reported.⁶⁰ Carbazolyl and dicyanobenzene groups are used as electron donor and acceptor, respectively. These molecules receive light energy from the lowest triplet state by spin up-conversion to the lowest singlet state owing to small energy gap between these states, which is useful for high ECL efficiency.

To examine the effect of structure, the ECL of a number of donor-acceptor type luminophores were also studied. A recently emerged report involved dithienylbenzothiadiazole-based red fluorophore [4,7-bis(4-(n-hexyl)-5-(3,5-di(1-naphthyl)phenyl)-thiophen-2-yl)-2,1,3-benzothiadiazole, **DBT**] in different states—solution, film, and nanoparticle.⁶¹ **DBT** has a donor-acceptor-donor configuration, which comprises a 2,1,3-benzothiadiazole moiety as the acceptor and two bulky substituted thiophene end groups as donor groups. Strong ECL was generated from **DBT** in different states by different pathways. **DBT** in solution produced strong ECL by annihilation, while **DBT** films and nanoparticles exhibited strong ECL in aqueous medium through a coreactant pathway. In addition, **DBT** film and nanoparticles exhibit both ~17 nm red-shifted absorbance and fluorescence emission spectra compared to those of **DBT** dissolved in solution. This is an interesting example to tune ECL of organic luminophores by changing states from liquid to solid phase.

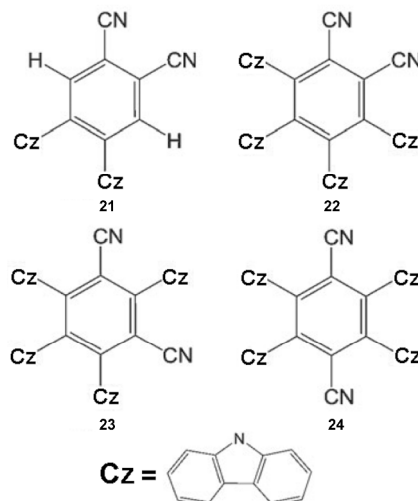


Fig. 13 Molecular structure of compounds **21–24**. Reprinted with permission from ref. 60.

In order to exploit the emission tunable system with higher quantum efficiency, three novel donor-acceptor luminophores (fig. 14) bearing triphenylamine groups as donor connected to fluorene, 2,7-bis(4-(N,N-diphenylamino)phen-1-yl)-9,9'-dimethylfluorene (**25**), or spirobifluorene core, 2,7-bis(4-(N,N-diphenylamino)phen-1-yl)-9,9'-spirobifluorene (**26**) and 2,2',7,7'-tetrakis(4-(N,N-diphenylamino)phen-1-yl)-9,9'-spirobifluorene (**27**), were synthesized.⁶² Upon tuning the emission by the donor, all the compounds display not only highly efficient blue emission upon photoexcitation but also intense ECL emission in the greenish blue region through both the coreactant (with benzoyl peroxide) and annihilation routes. Meanwhile, the ECL efficiency was higher than that of standard 9,10-

diphenylanthracene.

Interestingly, the ECL emission colors of organic luminophores are also tunable by changing coreactant molecules. A blue ECL of corannulene in acetonitrile was obtained by using both benzoyl peroxide and arylamine derivatives as mixed-annihilation coreactants.⁴⁰ In particular, by utilizing different tris(arylamine)s as mixed-annihilation coreactants, the emission colors could be tuned from green to blue, which opens a potential way to utilization corannulene and its derivatives for fabricating efficient blue-light emitting devices.

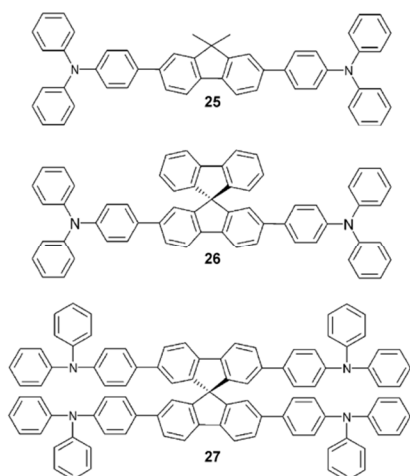


Fig. 14 Molecular structure of compounds 25-27. Reprinted with permission from ref. 62.

2.3 Nanoparticle systems

2.3.1 ECL nanohybrids

Since the ECL phenomenon of silicon nanoparticles was first reported in 2002, a series of quantum dots, including CdSe, CdS, CdTe, PbS, ZnSe, and Ag₂Se nanoparticles, have been reported.² For quantum dots based ECL, some excellent reviews have been published before,^{2, 12, 63, 64} so it will not be elaborated in detail here. Besides quantum dots, other miscellaneous nanomaterials with various compositions, sizes and shapes, such as graphite-like carbon nitride, metallic nanoclusters,^{65, 66} carbon nanodots,^{67, 68} and graphene and its composites,⁶⁹⁻⁷¹ have also been used as ECL emitters in recent years.

Greenish-yellow graphene quantum dot (QD) has been synthesized by a simultaneous cleaving and reduction process in the mixture of HNO₃ and H₂SO₄ using microwave treatment. It can be further reduced with sodium borohydride to generate blue graphene QDs with higher quantum yield. These graphene QDs was employed to demonstrate ECL of graphene QDs using potassium persulfate as the coreactant for the first time. The graphene QDs ECL allows selective and sensitive cadmium ion detection using cysteine as the masking agent, indicating that graphene QD is a promising ECL luminophore for ECL detection.⁷¹

Graphite-like carbon nitride has received considerable attention due to its special structure and properties, such as good chemical and thermal stability at ambient conditions, inexpensive and nontoxic, and facile synthesis. Recently, the ECL behavior of graphite-like carbon nitride was investigated, and the cathodic

and anodic ECL emissions were observed respectively.⁷²⁻⁷⁴ The possible ECL reaction mechanisms were proposed. For cathodic (or anodic) ECL, the electro-reduced (or electro-oxidized) graphite-like carbon nitride reacts with the intermediate generated from coreactant upon electrochemical reduction (or oxidation) to produce excited state graphite-like carbon nitride that subsequently returns to its ground state, emitting intense luminescence. Moreover, graphite-like carbon nitride was also employed to fabricate ECL sensor for detection of Cu²⁺ or rutin,^{72, 73} based on the effectively quenching of the ECL of graphite-like carbon nitride by them. These studies demonstrated that the nontoxic and inexpensive graphite-like carbon nitride could be a promising ECL luminophore in ECL sensor. Gold nanoparticles functionalized graphite-like carbon nitride nanohybrids which exhibit improved ECL stability and ECL intensity compared to graphite-like carbon nitride were also prepared and used to develop ECL immunosensor for detection of carcinoembryonic antigen (CEA).⁷⁵

Noble metal nanoclusters consisting of a few to tens of atoms have recently received considerable attention owing to their ultrasmall size (<2 nm), molecule-like behavior, desirable photophysical properties, facile synthesis, low toxicity and biocompatibility. So far, the applications of noble metal nanoclusters in analytical fields are mainly based on their fluorescence properties, and reports on the ECL properties of noble metal nanoclusters are scarce. Recently, the ECL of Au₂₅(SC₂H₄Ph)₁₈⁺-C₆F₅CO₂⁻ (Au₂₅⁺), Au₂₅(SC₂H₄Ph)₁₈⁻ (Au₂₅⁻), Au₃₈(SC₂H₄Ph)₂₄ (Au₃₈) and Au₈ clusters were reported successively. The near-infrared ECL emission of Au₂₅⁺ clusters was observed in the annihilation of electrogenerated Au₂₅²⁺ and Au₂₅²⁻ species and enhanced in the path of coreactant system with benzoyl peroxide for the first time.⁷⁶ By means of electrochemistry, photoluminescent spectroscopy, and newly developed spooling spectroscopy, the ECL mechanisms were explicitly elucidated as being due to the electronic relaxation of the Au₂₅^{*} excited state to the ground state across HOMO-LUMO gap. Compared with Au₂₅⁺, Au₂₅⁻ is more stable and relatively easy to prepare. The near-infrared ECL of the Au₂₅⁻ clusters was also observed by the same group.⁷⁷ Their study revealed that the Au₂₅⁻/TPA system was more efficient than the Au₂₅⁻/benzoyl peroxide. So far, the most efficient near-infrared ECL was attained from the Au₃₈/TPA coreactant system, which reached an efficiency of 3.5 times higher than that of the Ru(bpy)₃²⁺/TPA system.⁷⁸ In addition to near-infrared ECL, the ECL of metal nanoclusters in the visible region was also obtained. With organic-soluble fluorescent Au₈ clusters as the research object, both the annihilation ECL of fluorescent Au₈ clusters in organic solution and the coreactant ECL of fluorescent Au₈ clusters film in aqueous solution were observed.⁷⁹ With the advantages of less toxicity, high stability, and easier preparation, the fluorescent metal clusters may have potential applications in the future as a new ECL luminophore.

Despite that many nanomaterials-based luminophores have been developed, they generally have certain disadvantages, such as uneven size distribution, easy influence by structure, and great changes of luminescent properties after interaction with other substances. The combination of traditional light-emitting reagents with nanoparticles is a very promising way to develop new

efficient luminophores. Silica nanoparticles doped with two different dyes were prepared and applied in encoding ECL.⁸⁰ $\text{Ru}(\text{bpy})_3^{2+}$ was doped in the outer shell of silica nanoparticles as the red ECL emitter and fluorescein isothiocyanate was doped inside the shell as green fluorescent coding dye (fig. 15). When silica nanoparticles were exposed to light emitting diode exciting light and a potential of 1.3 V was applied to it, optical coding can be realized by ordinarily changing the molar ratio of co-doped dyes, which makes dual dye-doped silica nanoparticles promising ECL sensors in simultaneous determination of different analytes in a single sample.

Stimuli-responsive hydrogel nanoparticles (or microgels) are a kind of particularly fascinating nanomaterial, because their properties can be modulated by an external stimulus. However, examples of electrochemically active microgels have been reported rarely. The combination of ECL with stimuli-responsive microgels to design novel nanoparticles is attractive, because the ECL signal can be operated not only by the electrode potential but also by an external stimulus. Recently, the ECL of thermoresponsive redox microgels, synthesized by incorporation of ruthenium complex derivative into the thermo-responsive monomer with a cross-linker agent, was investigated by Sojic's group. Interestingly, ECL intensities change reversibly by reversibly changing temperatures, and an amplification of the ECL intensity up to 2 orders of magnitude in 100-nm thermoresponsive microgels is achieved.⁸¹ The reversible ECL enhancement is intrinsically correlated with the swell-collapse transition of the microgels. When temperatures increase, the thermoresponsive microgels collapse. The collapse of microgels shortens the distance between adjacent redox sites, favors the electron-transfer processes in the microgels, and thus increases ECL intensities. Such ECL enhancement related to the distance dependence offers the opportunity to develop tunable ECL resonance energy-transfer nanomaterials for multicolor emission.

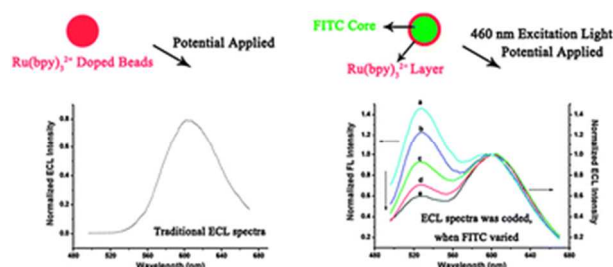


Fig. 15 Luminescent spectra comparison of $\text{Ru}(\text{bpy})_3^{2+}$ with $\text{Ru}(\text{bpy})_3^{2+}$ and fluorescein isothiocyanate dual dye-doped silica nanoparticles. Reprinted with permission from ref. 80.

Besides, in order to improve the ECL efficiency of luminol and its derivatives, luminol and iso-luminol functionalized gold nanomaterials,⁸²⁻⁸⁴ luminol functionalized $\text{Pt}@\text{Au}$ hybrid nanomaterials,⁸⁵ as well as luminol functionalized silver nanoparticles/graphene oxide composites⁸⁶ have been synthesized. These nanocomposites combine the advantageous properties of luminol, precious metal nanoparticles, and/or graphene oxide, and thus are promising platforms for multipurpose sensing and bioassays. The sensing platforms based on using these nanocomposites as the ECL signal probes show significantly enhanced ECL intensities and high sensitivities for target molecules.⁸⁵⁻⁸⁹

In addition to being used as ECL reagents, nanomaterials have also been extensively used as the electrocatalysts of ECL reactions. The properties of nanomaterials depend on their shape and size. However, most ECL nanocatalysts are a mixture of nanoparticles with different size and shapes, making it difficult to disclose the effects of sizes and shapes of nanocatalysts on ECL properties. Furthermore, noble metal nanocrystals with high-index facets are often catalytically more active than those with close-packed low-index planes because of their higher density of low-coordination-number step atoms, ledges and kinks. As a result, some efforts have been made on the shape-controlled and size-controlled synthesis as well as ECL studies of metal nanocrystals. $\text{Pd}@\text{Au}$ core-shell nanocrystals with different shapes including concave trisoctahedral,⁹⁰ tetrahedral⁹¹ and concave cubic⁹², and convex hexoctahedral with {431} high-index facets⁹³ (fig. 16) were synthesized and used to catalyze the ECL of luminol- H_2O_2 system. The nanocrystals showed much remarkable catalytic activity to the ECL of luminol- H_2O_2 systems.

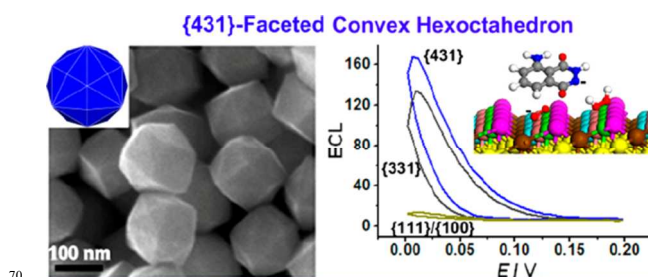


Fig. 16 SEM images of {431}-faceted convex hexoctahedron and ECL intensity-potential profiles of luminol/ H_2O_2 system on {431}-faceted convex hexoctahedral, {331}-faceted concave trisoctahedral, and {111}/100-faceted truncated octahedral $\text{Pd}@\text{Au}$ core-shell nanocrystal modified glassy carbon electrodes. Reprinted with permission from ref. 93.

2.3.2 Upconversion hybrid nanomaterials based ECL

Upconversion, also namely “anti-Stokes emissions”, is a process that converts a longer wavelength radiation, which are generally near-infrared light, into a shorter wavelength emissions (e.g., visible or UV) via a two-photon or multiphoton mechanism. Due to the unique properties, upconversion hybrid nanomaterials have attracted a lot of attention in a wide range of important electronic and biotechnological fields. However, the applications of upconversion nanomaterials in ECL fields remain rare. The electrogenerated upconverted emission in a uniformly doped organic nanowires based on triplet-triplet energy transfer from $\text{Ru}(\text{bpy})_3^{2+}$ to 9,10-diphenylanthracene was observed recently.⁹⁴ With the decrease in the molar ratio of $\text{Ru}(\text{bpy})_3^{2+}$ /9,10-diphenylanthracene from 1 : 3 to 1 : 10, the orange-red emission from $\text{Ru}(\text{bpy})_3^{2+}$ (at 540–640 nm) decreases sharply while the blue emission from 9,10-diphenylanthracene (at 380–500 nm) increases gradually. Since the triplet energy level of $\text{Ru}(\text{bpy})_3^{2+}$ is higher than that of 9,10-diphenylanthracene, the transformation from orange-red emission of $\text{Ru}(\text{bpy})_3^{2+}$ to blue emission of 9,10-diphenylanthracene indicates the triplet-triplet energy transfer from $\text{Ru}(\text{bpy})_3^{2+}$ to 9,10-diphenylanthracene and the relevant triplet-triplet annihilation based upconverted emission. This ECL upconversion system helps to avoid the interference from scattered light and luminescent impurities, which is an important advantage in applications including chemical or

biological sensing and imaging.

A graphene-upconversion nanohybrid material which exhibited a cathodic hot electron-induced ECL was also reported for the first time.⁹⁵ The graphene-upconversion nanocomposite was fabricated by a one-step *in situ* hydrothermal method, where the reduction of graphene oxide and the deposition of NaYF₄/Yb,Er on graphene occur simultaneously using graphene oxide as a precursor reagent. Compared with bare NaYF₄/Yb,Er nanoparticles, the ECL intensity of the graphene-upconversion nanocomposite was increased about 5-fold due to good electrical conduction and large specific surface area of graphene, which increased the possibility in future ECL-based applications. Soon after, a label-free, ultra-sensitive and selective ECL assay for detection of cyclin A₂ was developed by using the highly efficient ECL graphene-upconversion hybrid as a new luminophor.⁹⁶ The proposed assay showed a detection limit of 49.5 fM for cyclin A₂ in cell extracts.

2.3.3 Nanomaterials based ECL resonance energy transfer

In ECL resonance energy transfer, ECL reagent is used as an energy donor, and transfers the excitation energy of donor to the acceptor molecule, leading to the light emission from acceptor molecules. It has become a powerful technique for the sensitive detection of molecular interactions with a particular target molecule. In recent years, dye-quantum dot hybrids based ECL resonance energy transfer obtained more and more attention. Energy transfer mechanism between the Ru(bpy)₃²⁺/DBAE ECL system and quantum dots was investigated by Liu's group just recently.⁹⁷ It was found that the transfer mechanism between the Ru(bpy)₃²⁺/DBAE ECL system and quantum dots could be tuned by controlling the separation distances between them. When the separation distances between Ru(bpy)₃²⁺/DBAE system and QDs is much larger than the effective distance of charge transfer (<5.0 nm) and within the range of 50–100 Å, the ECL of the Ru(bpy)₃²⁺/DBAE system could transfer to quantum dots through ECL resonance energy transfer. In contrast, when the separation distances between Ru(bpy)₃²⁺/DBAE system and QDs were less than 5 nm, electron transfer played a major role in this hybrid system. This study provides a new way to tune ECL by distance.

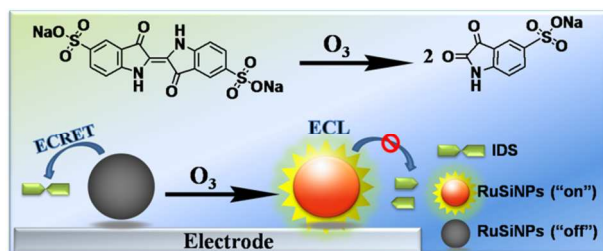


Fig.17 Scheme for the principle of ECL resonance energy transfer determination of ozone combined with RuSiNPs and indigo carmine. Reprinted with permission from ref. 98.

ECL emitter-doped silica nanoparticles are another kind of versatile materials for ECL resonance energy transfer. Ru(phen)₃²⁺-doped silica nanoparticles (RuSiNPs) was used as ECL sensor for sensitive detection of ozone via ECL resonance energy transfer (fig. 17).⁹⁸ ECL spectrum of RuSiNPs is overlapped with the absorption spectrum of indigo carmine at around 600 nm. Therefore, indigo carmine can quench the ECL

of RuSiNPs through the ECL resonance energy transfer of RuSiNPs to indigo carmine. Ozone can selectively decompose indigo carmine. Thus, ozone can interrupt ECL resonance energy transfer and increase the ECL signals. In this way the turn-on ECL detection of ozone was developed. RuSiNPs had also been utilized to develop ECL resonance energy transfer platform for detection of 2,4,6-trinitrotoluene (TNT).⁹⁹ In the presence of 3-aminopropyltriethoxysilane (APTES)-modified RuSiNPs, TNT can interact with APTES-modified RuSiNPs through strong acid-base pairing interaction to form a TNT-amine complex. The absorption spectrum of red color TNT-amine complex overlapped with the ECL spectrum of APTES modified RuSiNPs/triethylamine system. ECL intensity of APTES modified RuSiNPs/triethylamine system was quenched in the presence of TNT owing to resonance energy transfer from electrochemically excited RuSiNPs to the TNT-amine complex (fig. 18). This ECL resonance energy transfer method was successfully applied for the sensitive determination of TNT with the limit of detection of 0.3 nM within 1 min. Moreover, the ECL quenching method exhibited fine selectivity towards other nitro compounds including 2,4-dinitrotoluene and *p*-nitrotoluene.

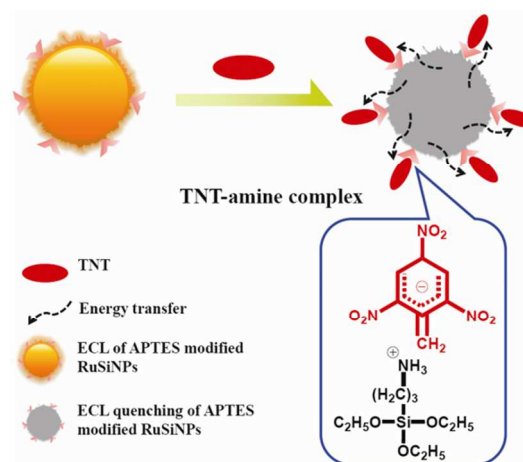


Fig.18 Schematic illustration of ECL turn-off detection of TNT by using APTES-modified RuSiNPs based on an ECL resonance energy transfer mechanism. Reprinted with permission from ref. 99.

3. ECL Analytical Applications

3.1 ECL immunoassay

One of the most important applications of ECL is its use in immunoassay. Compared with other techniques, the ECL technology has many distinct characteristics.^{3, 10} First, ECL possesses a very low detection limit (at subpicomolar concentrations) and an extremely wide dynamic range (greater than six orders of magnitude) for label detection. Second, the technique allows multi-parameter analyses by using ECL onset or peak voltages, ECL intensity, and wavelength. Third, the measurement is fast, because it requires only a few seconds. Fourth, no radioisotopes are used. Finally, only simple instrument is needed, and high-throughput analysis is allowed. Thus, the ECL immunoassay has become a powerful analytical tool for ultrasensitive detection of biomarkers.^{1, 3, 58, 100, 101} Over the past five years, many works have been done to improve sensitivity and extend applications of ECL immunoassays.

As a conventional ECL immunoassay, ECL enzyme linked immunosorbent assay was developed to detect cytosine methylation in DNA by using an antimethyl cytosine antibody labelled with acetylcholinesterase.¹⁰² This is the first report regarding the determination of methyl-cytosine in DNA by ECL, although the determination of DNA by ECL has been realized for several years. In this strategy, acetylcholinesterase converted acetylthiocholine (substrate) to thiocholine (product), which was a bifunctional molecule exhibiting both ECL acceleration effect and surface accumulation via gold–thiol binding (fig. 19). Owing to the accumulation and acceleration effect on ECL, methyl-cytosine was measured quantitatively in the 1–100 pmol range, which exhibits sufficiently high sensitivity to achieve real DNA measurements.

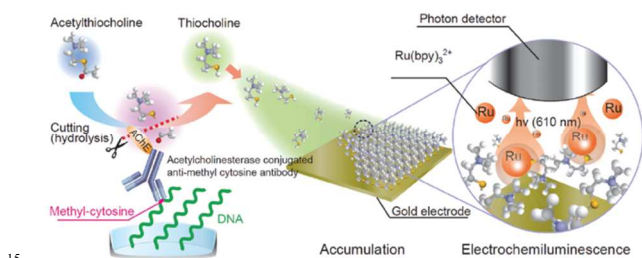


Fig. 19 Scheme for the principle of ECL determination of methyl-cytosine. Reprinted with permission from ref. 102.

Compared with the one-component detection, multi-component detection is more adapted to the needs of the clinical diagnosis. In order to achieve multi-component detection, a sandwich-type ECL immunosensor array with single-walled carbon nanotube forest microwells was reported.¹⁰³ As shown in fig. 20, single-walled carbon nanotube forests were surrounded by hydrophobic polymer to make microwells on the chip, then these upright, functionalized nanotubes offered a large conductive surface area for the attachment of capture antibodies of prostate-specific antigen and interleukin-6 in the bottoms of different wells. After incubation with the target proteins, silica nanoparticles containing Ru(bpy)₃²⁺ and secondary antibodies to prostate-specific antigen and interleukin-6 were added for highly sensitive two-target simultaneous detection. The ECL signals were measured with an inexpensive CCD camera, and the detection limits of 1 pg mL⁻¹ for prostate-specific antigen and 0.25 pg mL⁻¹ for IL-6 were obtained, which were equivalent to or better than commercial bead-based protein measurement systems.



Fig. 20 Schematic representation of ECL immunoarray. Reprinted with permission from ref. 103.

In order to enhance the luminous intensity of Ru(bpy)₃²⁺-based ECL system, a novel self-enhanced ECL luminophore of Ru(II) complex was developed by utilizing poly(ethylenimine) not only as coreactant but also form a novel coil-like nanocomposite with

bis(2,2' -bipyridine)-5-amino-1,10-phenanthroline ruthenium(II) [Ru(bpy)₂(5-NH₂-1,10-phen)²⁺]. On the basis of this self-enhanced ECL luminophore and sandwich-type ECL immunoassay, a signal on immunosensor for ultrasensitive detection of apurinic/aprimidinic endonuclease 1 was demonstrated for the first time, and the detection sensitivity was improved from pg mL⁻¹ to fg mL⁻¹.¹⁰⁴ Without adding of any other coreactant for signal amplification, the proposed immunosensor showed a detection limit of 0.3 fg mL⁻¹ for apurinic/aprimidinic endonuclease 1.

Compared with traditional laboratory testing, point-of-care diagnostic based on the development of miniaturized and portable analytical platforms is simple, rapid, and inexpensive. It has received growing interest owing to the fact that rapid biochemical assays can be performed directly where the sample is obtained, which meet the current requirements for clinical analysis and diagnosis.^{105–109} Very recently, a self-powered 3D microfluidic ECL biosensing platform based on the origami technique was developed for the first time (fig. 21).¹⁰⁶ In the proposed ECL biosensing device, a stable, environmentally-friendly and noble metal-free primary battery (C|FeCl₃|NaCl|AlCl₃|Al) was employed and used for driving the Ru(bpy)₃²⁺ ECL system with a very simple structure, which avoided the employment of expensive electrochemical workstations and promoted the miniaturization and further applications of the design. By assembling the energy part and the sensing part together in a 3D paper chip, a self-powered ECL biosensor was developed, and used to detect glucose to demonstrate the sensing function of the design. The proposed microfluidic origami ECL device exhibits broad applying prospect in point-of-care diagnostics. Interestingly, a low-cost and portable rechargeable battery, instead of expensive electrochemical workstation, was also developed as cost-effective and environmentally benign power supply to trigger ECL on a 3D microfluidic origami immunoassay electronic device, which is appealing for developing portable devices for point-of-care testing and on-site test.¹⁰⁷ Moreover, a home-made potential transformer has recently been employed, enabling the tuning of potential with cheap minidevices.¹⁰⁵

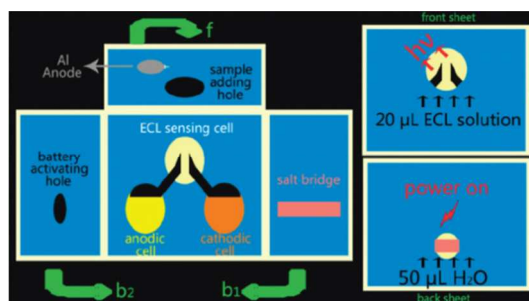


Fig. 21 Schematic illustration of the working principle of the self-powered 3D microfluidic ECL biosensing device. f: front sheet; b1: the sheet folded to the back first; b2: the back sheet. Reprinted with permission from ref. 106.

The mentioned above 3D microfluidic ECL biosensing platform achieve successfully detection of one target. In the following report, a multiple target pattern of 3D origami ECL immunodevice for sensitive and specific point-of-care diagnostics was developed based on a porous Ag-paper working electrode as a sensor platform and multi-labelled nanoporous gold–carbon spheres as tracers.¹⁰⁸ The fabricated porous Ag-paper working

electrode could not only immobilize antibody with good bioactivity, but also catalyze ECL systems $\text{Ru}(\text{bpy})_3^{2+}$ - H_2O_2 , luminol- H_2O_2 , and quantum dots- H_2O_2 for signal amplification. The developed immunodevice was used for near-simultaneous

detection of three cancer markers CEA, CA125, and AFP, with detection limits of 0.8 pg mL^{-1} , 1.2 mU mL^{-1} , and 1.0 pg mL^{-1} , respectively. Quantum dots-based near-infrared ECL immunosensors have also been developed in recent years.^{110, 111} Compared with quantum dots-based ECL in the visible range, near-infrared ECL has some attractive advantages including improved tissue penetration, lower background interference, and reduced photochemical damage. Recently, an immunosensor based on CdTe/CdS quantum dots near-infrared ECL was designed for the detection of target antigen with dual-signal amplification.¹¹⁰ Integrating the dual amplification from the accelerating electron transfer rate of gold nanoparticle-graphene nanosheet hybrids and the increasing quantum dot loading of functionalized SiO_2 nanospheres labels, a 16.8-fold enhancement near-infrared ECL response from CdTe/CdS quantum dots was obtained as compared to the unamplified protocol. With this strategy, the detection limit for human IgG was as low as 87 fg mL^{-1} . On this basis, a triply amplified ECL immunosensor based on gold nanoparticle-graphene nanosheet hybrids, $\text{Ru}(\text{bpy})_3^{2+}$ -encapsulated silicon nanoparticles and biotin-streptavidin was also developed for ultrasensitive detection of pseudorabies virus antibody with a detection limit of 0.40 pg mL^{-1} .¹¹²

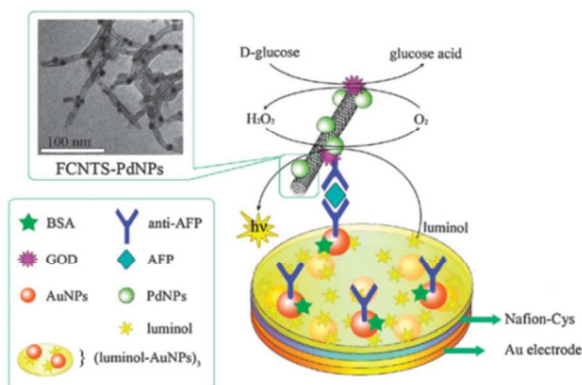


Fig. 22 Schematic diagram of the ECL-based sandwich-type immunosensor for detection of α -1-fetoprotein. Reprinted with permission from ref. 115.

Luminol based ECL has been widely used in immunoassay for a long time. The sensitivity of these immunoassays could be improved when nanoparticles were introduced.^{87, 113-116} A sandwich-type immunosensor based on the ECL of luminol with Pd nanoparticles and glucose oxidase as synergetic catalysts was proposed (fig. 22).¹¹⁵ In this study, Pd nanoparticle was used to immobilize glucose oxidase. It can not only retain the activity of glucose oxidase in the maximum degree owing to its good biocompatibility, but also catalyze the ECL reaction efficiently. The prepared immunosensor was successfully applied for the ultrasensitive detection of α -1-fetoprotein with a low detection limit of 33 fg mL^{-1} , which is lower than other sandwich-type methods. Besides Pd nanoparticles, ZnO nanoparticles was also utilized to construct sandwich-type luminol ECL immunosensor for CEA by using ZnO *in situ* generated H_2O_2 as coreactant.¹¹⁶

Due to the multiple signal amplification strategy, the ECL response of the fabricated immunosensor was greatly enhanced nearly 300 times. Compared with other methods of CEA immunoassay, the proposed ECL immunosensor exhibited higher sensitivity with a lower detection limit of 3.3 pg mL^{-1} CEA. In addition to conventional ECL reagents, peroxydisulfate based ECL immunoassay systems were also developed for sensitive detection of α -1-fetoprotein.^{117, 118}

3.2 DNA detection

Since the sensitive detection of DNA is of great importance in areas of medical diagnosis, environmental investigations, gene expression analysis, pharmaceutical studies, homeland security, and forensic analyses, ECL has been used as a powerful and important analytical technique for DNA detection. ECL DNA assays include two types of label-free and label ECL detection. Meanwhile, various amplification techniques including label and label-free have been used to improve the sensitivity of DNA detection. Compared with label ECL detection, label-free ECL detections possess the advantages of timesaving, low cost, simple manipulation and good reproducibility. By using *in situ* hybridization chain reaction signal amplification, a universal and highly sensitive strategy for label-free ECL detection of sequence specific DNA at the femtomolar level was described.¹¹⁹ The signal amplification relied on the hybridization chain reaction-induced formation of double-stranded DNA polymers on the sensing surface and the intercalation of massive ECL indicators ($\text{Ru}(\text{phen})_3^{2+}$) into the double-stranded DNA grooves (fig. 23). The developed method achieved comparable or even better sensitivity against some other common amplified DNA detection schemes. Later, another approach based on a supersandwich DNA structure and the intercalation of $\text{Ru}(\text{phen})_3^{2+}$ into double-stranded DNA as the ECL probe was used for the detection of DNA methylation and the assay of the methyltransferase activity.¹²⁰ This label-free ECL method is capable of detecting methyltransferase with a detection limit of $3 \times 10^{-6} \text{ U mL}^{-1}$.

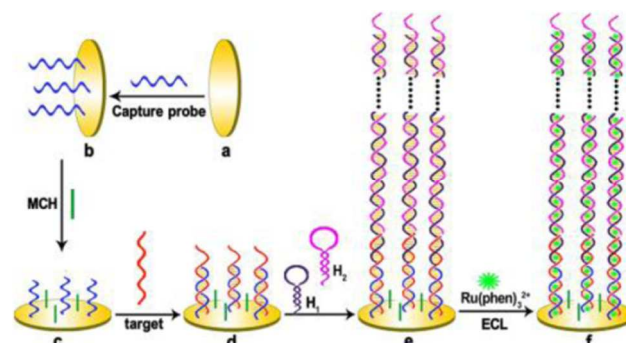


Fig. 23 Schematic representation of the preparation of the hybridization chain reaction-based ECL DNA sensor. Reprinted with permission from ref. 119.

In label ECL detection of DNA, Ru complex can be indirectly modified with nanoparticles or directly labelled with DNA. DNA-gold nanoparticle biobarcode assay has shown promise in the development of powerful tools for nucleic acid detection during the past decades owing to its unique non-enzymatic means of amplification. Recently, a series of sensitive methods based upon the combination of ECL and the DNA-gold nanoparticle biobarcode method for DNA detection have been developed.¹²¹⁻

¹²³ Typically, an ECL biobarcode assay was presented by using a novel ECL nanoprobe of gold nanoparticles modified with Ru(bpy)₃²⁺ labelled cysteamine to boost ECL signals and using single strand DNA for target recognition.¹²¹ A limit of detection as low as 100 fM is achieved and the assay exhibits excellent selectivity for single-mismatched DNA detection even in human serum. Besides gold nanoparticles, graphene oxide is another satisfied platform for nucleic acid detection owing to its excellent aqueous solubility and biocompatibility. Ru(II) complex functionalized graphene oxide (Ru-GO) has been successfully synthesized, and homogeneous ECL DNA sensor for the sensitive detection of *rpoB* genes of mycobacterium tuberculosis was developed by using Ru-GO as sensing interface and ferrocene labelled single-stranded DNA (Fc-ssDNA) as ECL intensity controller.¹²⁴ The ECL signal of Ru-GO can be effectively quenched by the Fc-ssDNA adsorbed on the Ru-GO nanosheets. Due to the good discrimination ability of graphene oxide over single-stranded DNA and double-stranded DNA, the target DNA can hybridize with Fc-ssDNA to form double-stranded DNA and release Fc-ssDNA from Ru-GO surface, resulting in the recovery of ECL. The designed strategy allows for detecting the target DNA with a detection limit of 0.04 nM. Moreover, the developed homogeneous DNA sensor is simple and rapid without immobilization procedures or separation and washing steps.

Ru(bpy)₃²⁺ derivatives can also be directly labelled with DNA to form ECL probe.^{125, 126} A signal-on DNA biosensor architecture was designed based on the ECL quenching of the Ru(bpy)₃²⁺ derivatives/TPA system by pristine multiwall carbon nanotubes.¹²⁵ In this strategy, single-stranded DNA labelled with Ru(bpy)₃²⁺ derivatives probe was wrapped around onto the multiwall carbon nanotubes, which makes ECL signals of Ru(bpy)₃²⁺ derivatives probe essentially quenched by the multiwall carbon nanotubes. In the presence of target DNA, the formed double-stranded DNA forced ECL probe away from the near surface of the multiwall carbon nanotubes, resulting in great enhancement of ECL signal. The developed approach allowed the sensing of the analyte DNA with a detection limit of 0.091 pM. It is the first report about ECL quenched by multiwall carbon nanotubes, which shows the great promise of multiwall carbon nanotubes in helping to decrease the background ECL signals for DNA detection.

Single molecule detection is the ultimate goal in chemical analysis. The investigation of single molecule is to observe the dynamic behavior of individual molecules, to explore heterogeneity between molecules, and to determine mechanisms of action, which allows for scrutiny of fundamental principles and mechanisms. ECL technology can also be used in developing ultrasensitive methods for near single molecule detection. An ultrasensitive ECL biosensor was developed for detection of near single DNA molecules with a linear range of 7 orders of magnitude by combining the specific recognition of a hairpin DNA molecular beacon with signal amplification of quantum dots-dendrimer nanocomposites.¹²⁷ The hairpin DNA molecular beacon was immobilized on a gold nanoparticles modified glassy carbon electrode. In the presence of target DNA, the molecular beacon hybridized with the target DNA and opened the beacon loop. Then quantum dots-dendrimer nanocomposites were covalently linked to the terminus of the beacon loop, resulting in

strong and stable ECL signals. The developed protocol integrated the specificity of a molecular beacon for molecular recognition to target analyte, the high loading of quantum dots by the dendrimer for ECL signal amplification, and the advantages of gold nanoparticles for immobilizing the molecular beacon on the electrode surface and accelerating the electron transfer. This strategy possessed promising potential in application to near single molecule detection of other kinds of biomolecules.

3.3 Functional nucleic acid sensors

With the rapid development of screening techniques, a large number of functional oligonucleotides such as aptamers and DNAzymes have recently been selected *in vitro*. Aptamers are single-stranded nucleic acids (DNA or RNA) with special functions that possess high recognition ability to a broad range of molecular targets including small molecules, ions, proteins, and even whole cells. Compared to traditional molecular recognition elements, aptamers exhibit many advantages including simple synthesis, good stability, easy storage, high affinity and specificity, and simple modification for further immobilization procedure, etc.

Owing to their unique properties, aptamers have attracted increasing interest as ideal recognition elements for ECL bioanalytical applications. After rapid development for several years, ECL aptamer detection has achieved a number of important progresses, and various aptamer-based ECL biosensing formats for the determination of proteins and small molecules have been developed. A protocol for ultrasensitive ECL detection of thrombin was presented based on layer-by-layer assembly of CdTe quantum dots onto the surfaces of the polystyrene microbeads as ECL signal amplification labels.¹²⁸ With this polystyrene-(CdTe)₂ labels, about 2–4 orders of magnitude improvement in detection limit for thrombin was obtained compared with that of other universal signal amplification routes. The detection limit could be pushed down further by increasing the number of CdTe quantum dot layer coated on the polystyrene beads.

ECL aptasensors for the detection of small molecules have also been reported. Quenching ECL of Ru(bpy)₃²⁺-doped silica nanoparticles by ferrocene was used to develop ECL aptasensors for the determination of adenosine.¹²⁹ A complementary DNA labelled with Ru(bpy)₃²⁺-doped silica nanoparticles was firstly immobilized onto the gold electrode surface. Then ferrocene-labelled aptamer was immobilized onto the gold electrode to form double-stranded DNA on the electrode surface through hybridization with complementary DNA, resulting in ECL quenching of Ru(bpy)₃²⁺-doped silica nanoparticles by ferrocene. In the presence of adenosine, ferrocene-labelled aptamer form preferentially adenosine-aptamer complex with adenosine and force ferrocene-labelled aptamer far away from the surface of electrode, which brings an increase ECL. Using this method a detection limit of 31 pM for adenosine was obtained.

Since labelling DNA aptamer involves complicated modification process, label-free ECL detection is extensively investigated owing to its advantages of simplicity. A label-free and sensitive ECL aptasensing scheme for K⁺ was developed,¹³⁰ which is based on the observation that the free state G-rich DNA aptamer can enhance the ECL signal of chitosan/Ru(bpy)₃²⁺/silica nanoparticles modified on electrode more effectively than its G-

quadruplex structure (binding with K^+). By using the decreasing ECL signals to detect K^+ , a detection limit of 0.3 nM K^+ was achieved. According to the detection mechanism, the proposed platform may be expanded to sensitively detect other targets.

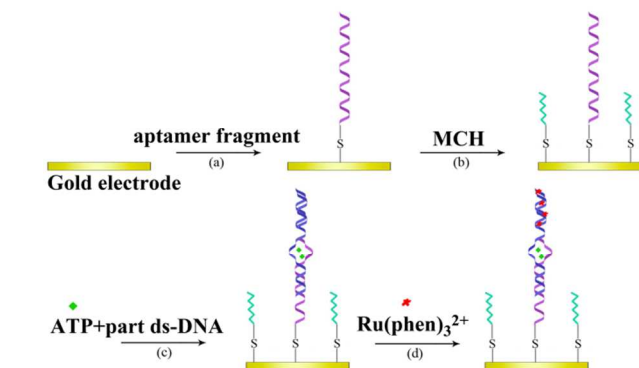


Fig. 24 Schematic representation of the label-free ECL-based aptasensor for detection of ATP. Reprinted with permission from ref. 131.

To further eliminate the complicated process for synthesis of ECL probe, such as $Ru(bpy)_3^{2+}$ -doped silica nanoparticles or chitosan/ $Ru(bpy)_3^{2+}$ /silica nanoparticles, a label-free sandwich-type ECL aptasensor by utilizing $Ru(phen)_3^{2+}$ intercalated into double-stranded DNA as ECL probe was reported based on target-induced conjunction of split aptamer fragments for highly sensitive detection of ATP.¹³¹ As shown in fig. 24, an anti-ATP DNA aptamer was divided into two different fragments which do not interact with each other in the absence of ATP. One fragment was immobilized on the gold electrode; the other one, lengthened with other 23-mer DNA sequence, was hybridized with its complementary single strand DNA to form a part DNA duplex. In the presence of ATP, a linkage of the immobilized aptamer fragment and part DNA duplex was induced to form strong aptamer-target complex on the electrode surface. Instead of the chemical modification of the aptamer or target with the probe molecule, $Ru(phen)_3^{2+}$ was intercalated into the double-stranded DNA structure as the probe. The increase in ECL intensity after the binding of ATP and its aptamer was used to quantify ATP. The intercalation of $Ru(phen)_3^{2+}$ into double-stranded DNA is a versatile protocol in developing label-free ECL aptasensors.

In order to extend the application of ECL probe intercalation to other systems, a label-free and “turn-on” supersandwich ECL biosensor for Hg^{2+} ions based on thymidine- Hg^{2+} -thymidine coordination was developed.¹³² In this protocol, two functional single-stranded DNA were designed with a thymidine-rich section for the recognition of Hg^{2+} ions, and could partially hybridize with each other forming an intermolecular duplex for $Ru(phen)_3^{2+}$ intercalation. In the presence of Hg^{2+} , thymidine- Hg^{2+} -thymidine coordination was formed between two functional single-stranded DNA, and then immobilized on the gold electrode, resulting in a great increase in ECL signal (fig. 25). Owing to the specificity of interaction between Hg^{2+} and multi-thymidine, and high sensitivity of supersandwich ECL detection, a detection limit of 0.25 nM was obtained.

Microfluidic paper-based analytical devices represent new and outstanding approaches to simple, portable, disposable, and low-cost devices for molecular analysis, environmental detection, and

health monitoring. In considerations of these advantages, a 3D microfluidic origami ECL aptamer-device for ATP was also developed based on a gold nanoparticle modified porous paper working electrode for point-of-care diagnosis.¹³³ The aptamer was successfully immobilized into the porous Au-paper working electrode as recognition elements. Phenyleneethynylene derivative modified nanotubular mesoporous Pt-Ag alloy nanoparticles were used as multi-labelling ECL labels to obtain amplified ECL signals. Due to dual amplification effects of the porous Au-paper working electrode and Pt-Ag alloy nanoparticles, the developed microfluidic origami ECL device showed a detection limit of 0.1 pM for ATP.

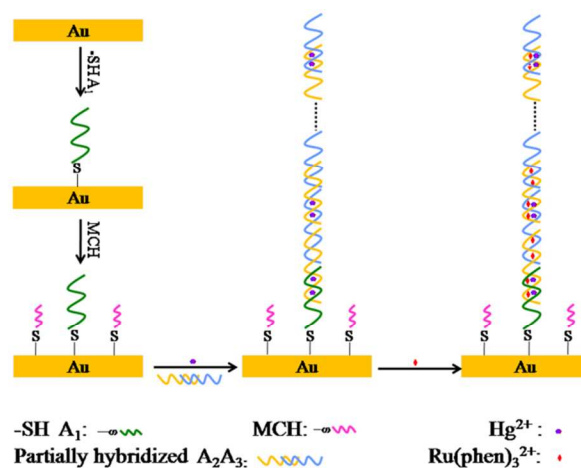


Fig. 25 Schematic diagram of the label-free supersandwich sensing platform for ECL detection of Hg^{2+} . (yellow curve, A2; blue curve, A3). Reprinted with permission from ref. 132.

Besides small molecules and proteins, ECL aptasensor has also been used for the detection of cells.¹³⁴⁻¹³⁶ An ultrasensitive hybrid bipolar electrode-ECL biosensor for the detection of cancer cell surface protein was proposed by using a ferrocene labelled aptamer as signal recognition and amplification probe.¹³⁶ The hybrid bipolar electrode used ITO glass as anode, and Au nanoparticles as cathode which can increase the cathodic current due to its excellent conductivity and large surface area. The increased cathodic current on Au nanoparticles resulted in an enhanced ECL of $Ru(bpy)_3^{2+}$ /TPA system on anode. Then, ferrocene labelled aptamer was introduced on the anode surface of bipolar electrode through hybridization with capture DNA at the anode. The oxidized species of ferrocene could quench the ECL intensity of $Ru(bpy)_3^{2+}$ /TPA system efficiently. In the presence of cancer cells, ferrocene labelled aptamer combined with target protein expressed on cell surface, resulting in a decreased number of ferrocene labelled aptamer hybridized with capture DNA at the anode. Coupled the cathodic Au nanoparticles induced ECL enhancing with the anodic ferrocene induced signal quenching amplification, the proposed approach allowed detection of cancer cell with a detection limit of 20 cells.

DNAzymes, also called catalytic DNA or deoxyribozymes, are DNA molecules that can catalyze many chemical and biological reactions. Since most reactions require specific metal ions as cofactors, it makes DNAzymes possess high metal-binding affinity and specificity towards metal ion. They are receiving growing interest as amplifying labels for sensing events and have

been implemented in numerous sensing platforms for the amplified detection of DNA, aptamer–substrate complexes, and metal ions, etc.^{137–140} For example, a specific ECL sensor for Pb²⁺ based on Pb²⁺-dependent DNazyme as a recognition element using intercalated Ru(phen)₃²⁺ as the ECL probe was designed.¹³⁸ Thiol-modified substrate was immobilized onto the surface of a gold electrode, and then hybridized with DNazyme to make a double-stranded DNA. Subsequently, the automatic intercalation of Ru(phen)₃²⁺ into double-stranded DNA proceeded. In the presence of Pb²⁺, the DNazyme catalyzed the hydrolytic cleavage of the substrate into two fragments, leading to the dissociation of DNazyme. Then the intercalated Ru(phen)₃²⁺ was released, resulting in the reduction of ECL intensity. The ECL intensity decreased with increasing Pb²⁺ concentrations in the range of 2 to 1000 pM. The detection limit for Pb²⁺ was 0.9 pM, which enabled analysis of trace amounts of Pb²⁺.

3.4 Solid-State ECL of Ru(bpy)₃²⁺ for detection of other species

Immobilization of Ru(bpy)₃²⁺ on the electrode to develop regenerable solid-state ECL sensors have attracted significant research interests, and many different methods and materials have been developed to immobilize Ru(bpy)₃²⁺.^{141–145} By exploiting electrospinning technique, a highly efficient solid-state ECL sensors was developed.¹⁴⁶ An electrospun poly (acrylonitrile-co-acrylic acid) nanofiber mat (PAN-co-PAA_{nfm}) was collected on the surface of a glassy carbon electrode, and the cationic luminescence probe Ru(bpy)₃²⁺ was first incorporated into the negatively charged PAN-co-PAA_{nfm}-modified glassy carbon electrode via electrostatic interaction. Compared with the Ru(bpy)₃²⁺ immobilized on normal PAN-co-PAA deposited coating, Ru(bpy)₃²⁺/PAN-co-PAA_{nfm} exhibited dramatically enhanced electrochemical and ECL performances, and more than 100 times higher ECL intensity was obtained via the electrospinning technique. The dramatically enhanced ECL of PAN-co-PAA_{nfm} modified electrode may attribute to the specific properties of electrospun nanofibers including good accessibility to the immobilized ruthenium complexes and easy permeation of the coreactant TPA, which allow TPA to be directly oxidized at the electrode surface and react efficiently with electrogenerated Ru(bpy)₃²⁺. In addition, the proposed Ru(bpy)₃²⁺/PAN-co-PAA_{nfm} modified electrode exhibited also the improved performance for detection of other analytes in aqueous solution.

Ru(bpy)₃²⁺ nanowires with large surface-to-volume ratios were prepared by solvent evaporation induced self-assembly and applied for the construction of ECL biosensor by immobilizing them onto a glassy carbon electrode with reduced graphene oxide-Nafion composite films.¹⁴⁷ The nanostructure of the Ru(bpy)₃²⁺ nanowires amplified the electro-active surface area of electrode, which improved the sensing property of the ECL sensor. The introduction of the reduced graphene oxide can significantly improve the conductivity of the Nafion film, and hence enhance the electrochemical signal of the Ru(bpy)₃²⁺ nanowires and increase its ECL intensity at low reduced graphene oxide concentration. The biosensor was used to detect dopamine with a low detection limit of 3.1×10^{-13} M.

Compared with Ru(bpy)₃²⁺, Ru(phen)₃²⁺ can be immobilized more easily because of its better adsorbability. A very simple method for immobilization of Ru(phen)₃²⁺ for ECL analysis was

presented just by mixing Ru(phen)₃²⁺ with graphite oxide to form Ru(phen)₃²⁺/graphite oxide precipitate.¹⁴⁸ The strong binding of Ru(phen)₃²⁺ with graphite oxide was attributed to the strong π - π stacking interaction and electrostatic interaction between them. The Ru(phen)₃²⁺/graphite oxide modified electrode was used to detect TPA with a detection limit of 3×10^{-7} mol L⁻¹.

4 Miscellaneous topics

4.1 Bipolar electrode-based ECL detection

After the first demonstration of ECL generation at the anodic pole of a bipolar electrode by Manz and co-worker in 2001,¹⁴⁹ ECL detection on bipolar electrodes has emerged as a sensitive, high-throughput, and low-cost approach for screening of electrocatalysts¹⁵⁰ and detection of analytes.^{151–155} Recently, a microfluidic ECL sensing platform based on a novel style of bipolar system with two-direction driving electrodes and dual-channel configuration was presented (fig. 26).¹⁵⁵ The bipolar electrode is smartly put between two channels, and thus a high current efficiency approaching 100% in theory was achieved. Moreover, the bipolar electrode anode were placed in the channel containing ECL probes, and the driving anode was in the channel without any ECL probe, enabling both the generation of intense ECL on the bipolar electrode anode and the complete elimination of background ECL signal on the driving electrodes. TPA, dopamine, H₂O₂, and K₃Fe(CN)₆ were detected by the device with good performance, which demonstrated that the proposed bipolar ECL sensing platform was promising in the real-time analysis of various targets.

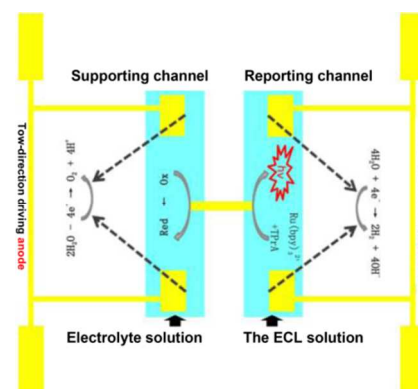


Fig. 26 Schematic illustration of the fundamental principle of the dual-channel bipolar ECL sensor. Reprinted with permission from ref. 155.

A low-cost, simple, portable, and disposable microfluidic paper-based electrophoretic device was also demonstrated by successful coupling with an electrophoretic separation technique and an on-column wireless ECL detector for the first time.¹⁵⁶ The introduction of electrophoretic separation technique has greatly improved the rapidness, repeatability, as well as sensitivity of the analytical device, and provided potential for multiplex separation and detection on microfluidic paper-based analytical device. Meanwhile, the utilization of wireless ECL detector allowed the fabricated analytical device more compact and simpler. Three amino acids (serine, aspartic acid, and lysine) were chosen as model analytes to investigate the construction and performance of the microfluidic paper-based electrophoretic device, capable of simultaneously performing electrophoretic separation and quantitative ECL determination. Results showed that it was a

powerful wireless detector which held great potential for the detection of other analytes through changing the electrode material and the external width of the η -shaped composite bipolar electrode.

Controlling and tracking the motion of small objects in real time is of crucial importance for many potential applications, and tremendous effort has been made to design particles with specific optical in recent years. An original approach was proposed based on bipolar electrochemistry and ECL.¹⁵⁷ When placing a conductive particle into an electric field, a polarization voltage produces between both terminuses of the particle. As shown in fig. 27, the asymmetric electroactivity induced by bipolar electrochemistry enables both the generation of hydrogen by the reduction of H_2O at cathodic pole and the generation of ECL by the oxidation of ECL reagents at the anodic pole, resulting in simultaneous motion and light emission from the bead in a glass capillary.¹⁵⁷ Directly monitoring of the motion of the object by ECL is very useful in the context of autonomous swimmers. Afterward, the ECL swimmer driven by bipolar electrochemistry was used for enzymatic glucose sensing for the first time.¹⁵⁸

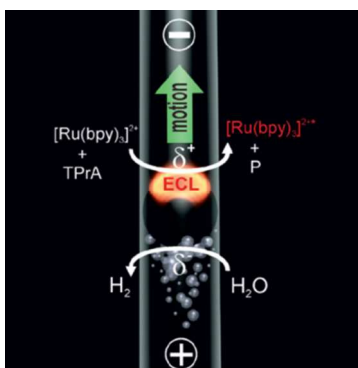


Fig. 27 Asymmetric light-emitting electrochemical swimmer. Reprinted with permission from ref. 157.

4.2 Wireless ECL

After the first demonstration of wireless energy transmission by Tesla more than 100 years ago, wireless energy transmission was broadly used in many aspects especially in wireless charging technology, but not in ECL analysis yet. Recently, wireless ECL system based on wireless energy transmission technique was developed for the first time.¹⁵⁹ The use of wireless energy transmission technique provided a facile way to avoid direct electrical contact of electrochemical instruments with any electrodes. As shown in fig. 28, the coiled energy receptor was used as the electrodes and a cheap wireless charging accessory of electric toothbrush or wireless power transmission module was utilized as a disposable transmitter. Wireless charging technology brings alternating potential and current, therefore ECL may occur alternatively on both electrodes and ECL color on two electrodes keeps nearly same. The wireless ECL system was used to detect H_2O_2 with good sensitivity. Owing to its easy manipulation, low cost, and small size, it was promising for the development of portable or disposable ECL devices for various applications including point of care testing, field analysis, scientific research, chemical education. More important, once integrated with screen printing coiled electrode arrays in microwell plates and CCD camera, this wireless ECL system can

be utilized to develop ECL high-throughput screening system in clinical analysis, drug screening and biomolecular interaction studying.

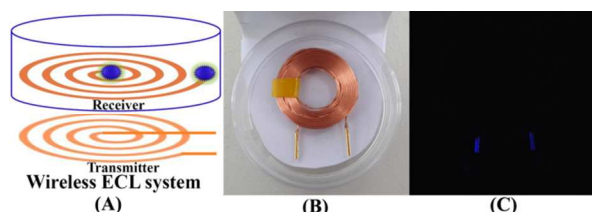


Fig. 28 Schematic diagram of the principle of the wireless ECL system (A), the photograph (B) and ECL image (C) of the wireless ECL minidevice based on utilizing two short gold wires connected with small lacquered copper coils in 50 mM Na_2CO_3 - NaHCO_3 buffer (pH 10.1) containing 50 mM H_2O_2 and 1 mM luminol. Reprinted with permission from ref. 159.

4.3 Scanning ECL microscopy

A noteworthy study appeared that scanning electrochemical microscopy was applied in investigating ECL of rubrene and $\text{Ru}(\text{bpy})_3^{2+}$ in the radical annihilation mode for the first time.¹⁶⁰ The scanning electrochemical microscopy tip was used as radical anion generator and the transparent, selectively insulated ITO substrate as the radical cation generator. Due to the simultaneous generation of steady-state radical ions in the microgap created between the scanning electrochemical microscopy tip and the transparent ITO substrate, a distance-dependent ECL signal was obtained, and some information about the light emission process, such as kinetics, stability, as well as mechanism, could be provided by the ECL signal. The ECL annihilation reactions, as probed by scanning electrochemical microscopy and ECL approach curves, were observed to follow very fast second-order homogeneous kinetics with an annihilation constant $k_{\text{ann}} > 10^7 \text{ M}^{-1} \text{ s}^{-1}$ for the case of the rubrene and $\text{Ru}(\text{bpy})_3^{2+}$ systems. Although it is quite challenging to implement the scanning electrochemical microscopy-ECL technique, the example of its use for two model systems, reveals that this technique has the potential application value in the clarification and understanding of ECL mechanisms.

4.4 Surface plasmon-coupled ECL

Surface plasmon resonance is a well-known technology based on light-metal thin film interactions. Recently, surface plasmon-coupled ECL based on solid-state ECL of immobilized $\text{Ru}(\text{bpy})_3^{2+}$ in Nafion was observed for the first time by coupling a hemispherical glass prism with $\text{Ru}(\text{bpy})_3^{2+}$ /Nafion modified gold film electrode.¹⁶¹ In surface plasmon-coupled ECL, energy radiates into the substrate at a defined angle. The ECL was efficiently collected from unoriented samples and directed towards a detector. Compared with solution-phase ECL based surface plasmon-coupled emission, solid-state ECL of $\text{Ru}(\text{bpy})_3^{2+}$ immobilized on the electrode surface possesses several advantages including saving expensive ECL reagent, simplifying experimental design, and increasing the ECL signal. These properties make solid-state ECL based surface plasmon-coupled emission useful for the analysis of chemical and biomolecular interactions.

Besides the use of surface plasmon resonance for efficient collection of unoriented ECL, surface plasmon resonance has also been utilized to achieve surface enhanced ECL of $\text{Ru}(\text{bpy})_3^{2+}$ utilizing localized surface plasmon resonance of nanostructured

materials, similar to surface enhanced Raman Spectrum (SERS). For example, surface enhanced ECL of $\text{Ru}(\text{bpy})_3^{2+}$ has been achieved with gold nanorods for the first time.¹⁶² DNA modified gold nanorods were immobilized on gold electrode. The binding of DNA with Hg^{2+} form hairpin structure which bring $\text{Ru}(\text{bpy})_3^{2+}$ closer to gold nanorods. Consequently, ECL was greatly enhanced with negligible current change and allows ultrasensitively detect Hg^{2+} . Surface enhanced ECL of $\text{Ru}(\text{bpy})_3^{2+}$ was also realized using gold nanoparticle- SiO_2 core-shell nanocomposites ($\text{AuNP}@\text{SiO}_2$).¹⁶³ It indicates that surface enhanced ECL based on surface plasmon resonance is promising in $\text{Ru}(\text{bpy})_3^{2+}$ ECL analysis.

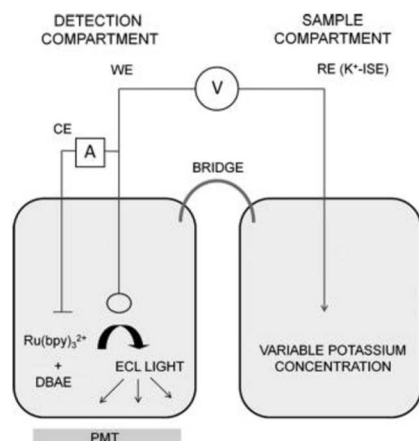


Fig. 29 Schematic representation of the electrochemical device with two separated sections (sample and detection) used to indicate the ECL readout conception for potentiometric sensors. Reprinted with permission from ref. 164.

4.5 Ion-selective electrode ECL

A unique optical ion sensor based on direct ECL output for potentiometric ion sensors has been demonstrated.¹⁶⁴ As shown in fig. 29, an applied potential between the gold working electrode and the potassium ion-selective electrode reference electrode produces the oxidation of $\text{Ru}(\text{bpy})_3^{2+}$ and DBAE, generating light at the gold electrode. The light is then collected with a photomultiplier tube placed outside the detection compartment. The potential at the working electrode is directly modulated by the changes in the sample potassium concentration, and hence change the ECL output. A linear response of the ECL intensity to the logarithmic potassium concentration between 10 μM and 10 mM was found. It is the first direct optical readout potentiometric sensor, and possesses the key advantages of without the requirement of a classical light source and without the need for a reference ion (typically the hydrogen ion) that has hampered the practical utility of these optical sensors if the reference ion activity is not accurately controlled or measured.

4.6 A Numerical Approach for the Simulation of ECL

ECL involve in heterogeneous electrode processes on the electrode surfaces and subsequent homogeneous chemical reactions of electrogenerated products in the solution. To generate ECL, extremely rapid second-order reactions occur in the diffusion layer followed by a very fast first-order emissive decay, resulting in the very low concentrations of the emitting species. Numerical methods with an excellent precision and accuracy are thus required for simulating ECL reaction

mechanisms and kinetics.¹⁶⁵ DigiSim and multi-purpose finite-element method software are popular simulation tools in the electrochemical community. DigiSim, which is a finite-differences-based program, relies on exponential spatial compression near an electrode surface to increase the precision in computing currents when thin kinetic layers form near the electrode over dimensions much smaller than the time-expanding diffusion layer. Since the critical kinetic layer in ECL locates far from the electrode and move with time (reaction front), the application of DigiSim in ECL simulation is very limited.¹⁶⁶ Multi-purpose finite-element method software was not designed to handle the very specific electrochemical boundary and kinetic conditions readily. It requires solid expertise from their potential users and may easily lead to erroneous predictions in the hands of novices. The combination of specialized electrochemical software and multi-purpose finite-element method software provide an alternative way for the simulation of ECL reaction mechanism, for example, Sartin et al. has indirectly evaluate ECL emission intensity by simulating voltammetric responses with DigiElch software and the concentration distributions of light-emitting species with Comsol software.¹⁶⁷

Impressively, Amatore et al. have developed a new numerical approach implemented in multi-purpose KISSA software (<http://kissagroup.com/>).^{165, 168-171} The approach based on the simultaneous implementation of specific conformal mappings of the space to adapt simulation grids to the characteristic problem imposed by the specific geometry of the working electrode and of a specifically developed kinetic criterion for adaptive tracking of rapid concentration changes and/or fronts of fast homogeneous reactions. The implementation is automatic and does not require specific decisions from the user, except defining the electrochemical system and a sequence of redox and chemical steps. KISSA based on the approach produces numerical solutions matching well with the corresponding analytical values for common ECL conditions. It allows fast, precise and efficient simulation and prediction of ECL reactions without the necessity of any particular computer or mathematical skills on part of the user. It is particularly advantageous to non-mathematically oriented electrochemical users in comparison with existing software and approaches. The KISSA software has thus recently been employed to simulate transition metal(II) /amine ECL systems. The study shows that the diffusion rates of reactants have strong effect on ECL and the ECL intensities of the first ECL wave would greatly increase by decreasing the diffusion coefficients of metal complexes species vs. that of the amine co-reactant. This finding is particularly important in search of new ECL systems for immunoassays and DNA detection where the first ECL wave plays critical role for detection.¹⁷²

4.7 Light-emitting electrochemical cells (LECs)

As a particular class of light-emitting devices, LECs are promising with novel features and the possibility of application to displays. The first solid state LEC was prepared by mixing with the electrolyte in the active layer of light-emitting diode in 1995. The major difference between LECs and light-emitting diode is the different operational mechanism, where mobile ions play a leading role in LECs while the operational mechanism of light-emitting diode is dominated by the holes and electronic

transmission in the multilayer device structures. Compared with light-emitting diode, LECs possess several advantages, such as simple device structures, low operating voltages, high luminescence quantum efficiency, and relative insensitivity to the electrode work function as well as to the film thickness of active layers. On the other hand, the shortages of LECs in the stability, lifetime, and brightness result in some limitations for practical applications. Therefore, extensive efforts have been made to overcome these. According to the type of luminescent materials used, LECs can be divided into two main classes, including polymer-based LECs and ionic transition-metal complexes (iTMCs)-based LECs.

4.7.1 Polymer-based LECs

For polymer-based LECs, the active layer composition is one of the fundamental factors that determine the device performance. To improve the performance of the device, many attempts have been made in optimizing the composition of the active layer. By increasing the concentration of the ion incorporated in the active layer, linearly increased current density and light emission were obtained over a wide range of concentrations owing to the enhanced conductivity of the active layer by electrochemical doping.¹⁷³ Hence, it can be concluded that the ion concentration should be as high as possible in the absence of detrimental side reactions and doping-induced luminescence quenching. Due to the superior electron transfer property and good structural stability of π -conjugated polymer, a polymer LEC with improved luminescence properties was fabricated using π -conjugated polymers poly(3-octylthiophene-2,5-diyl) as emitting material in the active layer.¹⁷⁴ A threshold voltage of as low as 2.4 V and long luminescence for about 6000 s were obtained from the ECL device. The luminescence time was longer than that of the LECs using ruthenium complexes.

By changing the active layer composition, the colors of the LECs can also be tuned. For color tuning, white light emission are very important due to the great demands in a wide range of current and futuristic display and solid-state lighting applications. The most usual enabling approaches used for the realization of broadband white emission are the utilization of a multilayer geometry containing stacked layers of complementary emitting materials or a single-layer geometry comprising an incorporated multicomponent emitter system. In comparison, single-component white LECs possess relatively easier fabrication processes. Recently, a single-layer single-emitter white LEC was reported by employing a multifluorophoric conjugated copolymer as the emitter and an electrolyte designed to inhibit energy-transfer interactions in the active layer.¹⁷⁵ Via inhibiting the energy transfer between the blue-emitting and red-emitting chromophores in multiple-chromophore copolymers by the electrolyte, white emission was produced. Besides, single-component salt-free white LEC was also fabricated by using polyfluorene electrolytes bearing hexafluorophosphate counterions as active layer.¹⁷⁶ The prepared single-component LEC device exhibits pure white light emission with a maximum luminescence efficiency of 1.56 lm W^{-1} , which is among the highest reported for white-light polymer LECs.

The electrode material is another important factor affecting the performance of LECs. Al, Ca, Au and ITO are commonly used electrode materials, wherein ITO is the most commonly used.

With the scarcity of indium resources, various materials have also been explored to replace ITO, such as using silver nanowires to prepare flexible transparent electrode material,¹⁷⁷ by use of single-walled carbon nanotubes to fabricated highly distorted light-emitting device,¹⁷⁸ and exploiting graphene as the electrode material to develop flexible and metal-free LECs.¹⁷⁹ These alternative electrode materials possess the advantages of flexible, low cost, and abundant resources.

The light-emitting p-n junction in LECs, also called frozen junction, is formed via *in situ* electrochemical doping. The off-center p-n junction is a major drawback in LECs, which results in exciton quenching at the electrode, and is harmful to the lifetime and efficiency of LECs. Hence, a lot of efforts have been devoted to move or define the p-n junction toward the center in between the two electrodes. By combining with the characteristics of LECs and organic electrochemical transistors, a three-electrode device, the light-emitting electrochemical transistor, was fabricated based on a bilayer LEC and a gate electrode.¹⁸⁰ The bilayer LEC was fabricated by separately stacking light-emitting polymer material and ion-conductive electrolyte onto two bottom electrodes. An electrochemically active conducting polymer material was then deposited on top of the bilayer LEC as a gate electrode. In the light-emitting electrochemical transistor, the emitting p-n junction was established between two bottom electrodes, and *in situ* controlled by the top gate electrode within an interelectrode gap of 500 μm , which potentially offered the possibility of modulating the light output characteristics. Nevertheless, the curvy shape and inhomogeneous lighting profile make it not very valuable in a practical application. To overcome these shortages, a double-gate light-emitting electrochemical transistor was constructed.¹⁸¹ Similar to its predecessor, the device also included a bilayer LEC. In addition, two gate electrodes were deposited onto the top of the bilayer LEC. In the double-gate light-emitting electrochemical transistor, a localized p-n junction precisely defined by two electrochemical gate electrodes with a more uniform profile was achieved.

4.7.2 iTMC-based LECs

Compared with polymer-based LECs, iTMC-based LECs possess simpler process of device fabrication and free from the problem of phase separation because of no additional electrolyte or ion-conducting material are needed in the device. Moreover, iTMC-based LECs generally have higher efficiency and brightness than polymer-based LECs owing to the efficient phosphorescence of iTMCs at room temperature. These advantages have made iTMC-based LECs obtain increasing attention. Several excellent reviews, especially the review published in 2012,¹⁸² have appeared and covered the development of iTMC-based LECs. Herein, only the latest and significant advances of iTMC-based LECs will be illustrated.

In order to extend the applicative potential of iTMC-based LECs for lighting and display technologies, which require wider color tunability, considerable efforts have been made to tune the light emission wavelength of iTMC and corresponding LECs. In three primary colors, blue light is very important, but blue-emitting iridium complexes are lacking. By using 1,2,3-triazole-pyridine as ancillary ligands in cationic iridium complexes, blue emission with maximum wavelength ranging from 460 to 490 nm was obtained and corresponding LECs with fast turn-on time

were fabricated.¹⁸³ Besides blue ECL emission, orange-red to deep red ECL emission with a maximum wavelength ranging from 680 to 722 nm and luminance up to 135 cd m⁻² was observed upon electrochemical switching of the polymeric networks by introducing both electron-withdrawing and -donating substituents into the acrylate-containing Ru(bpy)₃²⁺-based coordination complexes (fig. 30),¹⁴ although the color tuning of ruthenium complexes is difficult due to the limited ligand-field splitting energies of central metal ions of ruthenium complexes and most of ruthenium complexes exhibit orange-red emission with a maximum wavelength between 600 and 650 nm. Meanwhile, a dual electrochromic/electroluminescent device prototype based on the acrylate-containing ruthenium complexes was presented where light emission and multicolor electrochromism occur from the same pixel comprised of a single active layer, demonstrating a true combination of these properties in iTMC.¹⁴ The developed dual electrochromic/electroluminescent device not only can emit light in dark ambient lighting situations, but also can change its colored states when sufficient ambient light is available for a reflective mode, which allows for optimizing the visibility in any ambient lighting situation. The results also revealed that the pendant acrylate moieties crosslinkable ruthenium complexes were attractive candidates for well-defined dual electrochromic/electroluminescent active layers. To fabricate light emission color tunable LECs, a block-copolymer-based emissive ECL ion gel containing Ru(bpy)₃Cl₂ as the luminophore was demonstrated and used to construct flexible ECL devices for the first time (fig. 31).¹⁸⁴ The red-orange ECL devices with a simple sandwich configuration were fabricated on indium tin oxide-coated substrates by solution-casting the ECL gel and brush-painting a top Ag electrode. The fabricated ECL devices showed a low-voltage operation (VPP = 2.6 V, i.e., -1.3 to +1.3 V) and a rapid response time (sub-ms). By employing another luminophore Ir(diFppy)₂(bpy)PF₆, the emitting color of the ECL devices can be tuned to green. Moreover, remarkably enhanced red-orange-colored ECL in ion gels was achieved for the first time by using a mole ratio of 60:40 mixture of Ru(bpy)₃²⁺ and Ir(diFppy)₂(bpy)⁺ in the emissive layer and utilization of Ir(diFppy)₂(bpy)⁺* as a coreactant via the coreactant pathway apart from the usual annihilation pathway. All of the results indicated that ECL ion gels are attractive multifunctional materials for flexible electronics applications.

Due to the potential applications in solid-state lighting, white LECs have attracted much attention. To obtain white light, the simultaneous presence of complementary emitting colors is essential, which are usually blue and yellow. However, white LECs are less, which may be attributed to the lack of stable and deep-blue-emitting complexes that manipulate in a LEC device configuration. Unprecedented, an efficient phosphorescent sensitized white LEC without employing saturated deep-blue emitting iTMCs was obtained by doping a blue emitting phosphorescent iTMC with a red-emitting fluorescent dye.¹⁸⁵ Through suppressing the green part of the electroluminescence spectrum of the blue-green-emitting phosphorescent iTMC by the microcavity effect of the LEC structure, more saturated blue emission was obtained, enabling white emission by the combination of the saturated blue emission with saturated red

emission. To further improve the color stability of white LECs, a single-layered blue-emitting LEC were combined with red-emitting color conversion layers for construction of efficient and color-stable white LECs.¹⁸⁶ By choosing suitable red-emitting dye doped in color conversion layers, the color stability and the emission efficiency of the white LECs were increased significantly and among the highest reported for white LECs. In order to develop more highly efficient solid-state white LEC, double-doping strategy was also employed. Both an orange emitting guest, [Ir(ppy)₂(dasb)]⁺(PF₆⁻), and a red emitting guest, [Ir(ppy)₂(biq)]⁺(PF₆⁻), were introduced into an emissive layer containing an efficient blue-green emitting host, [Ir(dfppz)₂(dtb-bpy)]⁺(PF₆⁻), where ppy is 2-phenylpyridine, dasb is 4,5-diaza-9,9'-spirobifluorene, biq is 2,20-biquinoline, dfppz is 1-(2,4-difluorophenyl) pyrazole, and dtb-bpy is [4,4'-di(*tert*-butyl)-2,2'-bipyridine].¹⁸⁷ Due to the enhanced balance of carrier mobilities of the double-doped host-guest films, the device efficiencies of the double-doped white LECs were double higher than those of the single-doped white LECs. Besides, a novel white LECs based on a tandem structure was reported very recently.¹⁸⁸ By using a blue polymer-composite LEC as the bottom device and an orange iTMC-based LEC as the top device, white light was attained with a current efficiency of 8.5 cd A⁻¹ at a luminance of 845 cd m⁻².

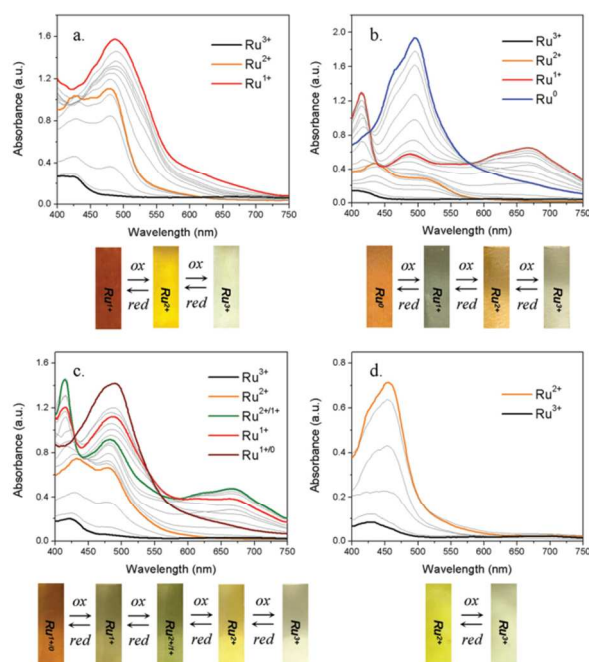


Fig. 30 Spectroelectrochemistry data and the corresponding photos of the polymeric films of **1** (a), **2** (b), **1** and **2** mixture in 1:1 molar ratio (c), and **3** (d) at all the unequivocally stable redox states in 0.1 M tetrabutylammonium hexafluorophosphate acetonitrile solutions. Structure of the acrylate-containing Ru(bpy)₃²⁺-based coordination complexes **1**, **2**, and **3** were shown in fig. 2. Reprinted with permission from ref. 14.

Besides color tuning, to improve the efficiencies of iTMC-based LECs is another important research interests for researchers. The efficiency has been significantly improved through increasing the intersite distance between the cations in the film by introducing bulky side groups of increasing size into iridium complexes.¹⁸⁹ An alternative way for improving the efficiency of near-infrared LECs device was established by using

phosphorescent sensitized fluorescence combined with a tandem device structure.¹⁹⁰ The tandem LECs device with a simple sandwich structure was fabricated by vertically stacking two identical emissive single-layers via a thin transporting layer. The emissive single-layer consisted of a phosphorescent host Ru(dtb-bpy)₃(PF₆)₂ (where dtb-bpy is 4,4'-ditertbutyl-2,2'-bipyridine) doped with a fluorescent ionic near-infrared dye 3,3'-diethyl-2,2'-oxathiocarbocyanine iodide. A thin poly(3,4-ethylenedioxythiophene):poly(styrene sulfonate) layer was used as the connecting layer. Due to the improved carrier balance of the tandem device induced by the connecting layer with a high electron injection barrier, an over tripled enhancement external quantum efficiency was obtained in tandem LECs as compared to previously reported near-infrared LECs based on the same near-infrared dye without the tandem device structure,¹⁹¹ which indicated that tandem device structure would be useful for enhancing device efficiencies of phosphorescent sensitized fluorescent near-infrared LECs.

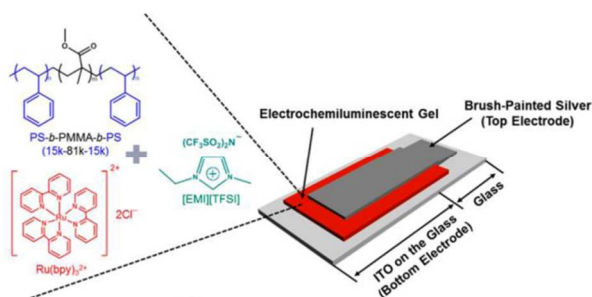


Fig. 31 Schematic representation of an ECL device based on an ECL emissive gel layer consisted of Ru(bpy)₃Cl₂/PS-b-PMMA-b-PS/[EM][TFSI] in the weight ratio 1:4:16 and a brush-painted top Ag electrode. Reprinted with permission from ref. 184.

Currently, another key limitation for the practical applications of iTMC-based LECs is their low stability. Much work has been done to improve the lifetime of iTMC-based LECs. By the use of an ionic iridium complex ([Ir(dmppz)₂(pbpy)][PF₆], incorporating 3,5-dimethyl-1 phenylpyrazole (Hdmppz) and 6-phenyl-2,2'-bipyridine (pbpy) as ligands) that forms a supramolecular cage via an intramolecular π-π stacking as the active component, the lifetimes of the LECs were significantly improved and reached around 2000 h at an applied bias of 3 V.¹⁹² The reason for the higher stability of the so-prepared LECs was attributed to the formation of supramolecular cage¹⁹³⁻¹⁹⁵ and the position of the pendant methyl groups of the dmppz ligands located over the octahedral faces, which make it more difficult for nucleophiles to attack the complex and then inhibit the degradation of the ionic iridium complexes. In another research, owing to the formation of intramolecular cage in the ionic iridium complex and the additional presence of a pendant protective phenyl group within the ancillary ligand, the stability of a blue-green LECs based on the complex was dramatically enhanced and reached a half-lifetime of 950 minutes at 3 V, which is much larger than those of other reported blue or blue-green LECs (several to tens of minutes).¹⁹⁶ The concept of supramolecular cage formation was also extended to a phenanthroline-based ionic iridium complex [Ir(ppy)₂(pphen)][PF₆] (Hppy = 2-phenylpyridine, pphen = 2-phenyl-1,10-phenanthroline). The lifetime of the LECs using the complex [Ir(ppy)₂(pphen)][PF₆] reached 230 h at an applied bias

of 3 V, which is three times higher than that measured in LECs using complex [Ir(ppy)₂(phen)][PF₆].¹⁹⁷

Although LECs with high efficiencies or excellent stabilities have been obtained separately, LECs simultaneously exhibiting both high efficiencies and excellent stabilities have rarely been reported. To make the LECs more stable, one effective and widely accepted way is to make the iTMCs more hydrophobic and difficult to breakdown. By modifying the ionic iridium complex [Ir(ppy)₂(bpy)][PF₆] via incorporating methyl groups on the 6-positions of the bpy ligand and two added bulky shielding groups on the 4 and 4' positions, more hydrophobic ionic iridium complexes with high photoluminescent quantum yields above 70% were obtained.¹⁹⁸ LECs using these complexes also show a high stability and efficiency.

5. Conclusions

ECL has established itself a powerful tool for ultrasensitive detection of a wide range of analytes and for understanding fundamental questions in chemistry, biology, and physics. More and more scientists study ECL, and more and more papers publish year by year, indicating that ECL is an area of active research. New ECL systems, such as nanomaterial systems, upconversion ECL systems, and resonance energy transfer ECL systems, will continue to attract much attention. Their corresponding mechanism and applications will be investigated. The development of ECL high-throughput assays based on microwell plate, bipolar electrochemistry, and wireless system and point-of-care testing with high sensitivity and good stability will continue. The broad clinical application of ECL will facilitate new analytical applications, such as food safety, water safety, and environmental monitoring applications. New ECL microchips and light-emitting devices will be designed. The combination of ECL with other techniques may appear to meet other research needs.

Acknowledgements

This work is kindly supported by the National Natural Science Foundation of China (No. 21475123 & 21175126), Chinese Academy of Sciences (CAS).

Notes and references

- ^a State Key Laboratory of Electroanalytical Chemistry, Changchun Institute of Applied Chemistry, Chinese Academy of Sciences, Changchun, Jilin 130022, People's Republic of China
- ^b University of the Chinese Academy of Sciences, Chinese Academy of Sciences, No. 19A Yuquanlu, Beijing 100049, China
E-mail: guobaoxu@ciac.ac.cn; Fax: +86-431-85262747; Tel: +86-431-85262747
- * Corresponding author: Prof. G. B. Xu
‡ Equal contribution.
- W. Miao, *Chem. Rev.*, 2008, **108**, 2506-2553.
 - J. Lei and H. Ju, *TrAC-Trend. Anal. Chem.*, 2011, **30**, 1351-1359.
 - L. Hu and G. Xu, *Chem. Soc. Rev.*, 2010, **39**, 3275-3304.
 - in *Electrogenerated Chemiluminescence*, ed. A. J. Bard, Marcel Dekker, New York, 2004.
 - H. Wei and E. Wang, *Luminescence: the journal of biological and chemical luminescence*, 2011, **26**, 77-85.

6. X. Chen, B. Su, X. Song, Q. Chen, X. Chen and X. Wang, *TrAC-Trend. Anal. Chem.*, 2011, **30**, 665-676.
7. J. Suk and A. J. Bard, *J. Solid State Electrochem.*, 2011, **15**, 2279-2291.
8. J. Li, S. Guo and E. Wang, *RSC Advances*, 2012, **2**, 3579-3586.
9. S. Deng and H. Ju, *Analyst*, 2013, **138**, 43-61.
10. K. Muzyka, *Biosens. Bioelectron.*, 2014, **54**, 393-407.
11. S. Zhang, Y. Ding and H. Wei, *Molecules*, 2014, **19**, 11933-11987.
12. P. Bertocello, A. J. Stewart and L. Dennany, *Anal. Bioanal. Chem.*, 2014, **406**, 5573-5587.
13. L. Ge, J. Yu, S. Ge and M. Yan, *Anal. Bioanal. Chem.*, 2014, **406**, 5613-5630.
14. E. Puodziukynaite, J. L. Oberst, A. L. Dyer and J. R. Reynolds, *J. Am. Chem. Soc.*, 2012, **134**, 968-978.
15. L. D. Ciana, S. Zanarini, R. Perciaccante, E. Marzocchi and G. Valenti, *J. Phys. Chem. C*, 2010, **114**, 3653-3658.
16. Y. Tian, S. Han, L. Hu, Y. Yuan, J. Wang and G. Xu, *Anal. Bioanal. Chem.*, 2013, **405**, 3427-3430.
17. Y. Yuan, S. Han, L. Hu, S. Parveen and G. Xu, *Electrochim. Acta*, 2012, **82**, 484-492.
18. Y. Zu and A. J. Bard, *Anal. Chem.*, 2000, **72**, 3223-3232.
19. S. Senthil Kumar and A. J. Bard, *Anal. Chem.*, 2013, **85**, 292-295.
20. W. Miao, J.-P. Choi and A. J. Bard, *J. Am. Chem. Soc.*, 2002, **124**, 14478-14485.
21. M. Sentic, M. Milutinovic, F. Kanoufi, D. Manojlovic, S. Arbault and N. Sojic, *Chem. Sci.*, 2014, **5**, 2568-2572.
22. Y. Yuan, H. Li, S. Han, L. Hu, S. Parveen and G. Xu, *Anal. Chim. Acta*, 2011, **701**, 169-173.
23. L. Hu, J. Gao, Y. Wang and G. Xu, *Anal. Methods*, 2011, **3**, 1786-1789.
24. L. Hu, H. Li, S. Han and G. Xu, *J. Electroanal. Chem.*, 2011, **656**, 289-292.
25. W. Qi, M. T. Gabr, Z. Liu, L. Hu, M. Han, S. Zhu and G. Xu, *Electrochim. Acta*, 2013, **89**, 139-143.
26. W. Qi, Z. Liu, J. Lai, W. Gao, X. Liu, M. Xu and G. Xu, *Chem. Commun.*, 2014, **60**, 8164-8166.
27. G. J. Barbante, E. H. Doeven, E. Kerr, T. U. Connell, P. S. Donnelly, J. M. White, T. Lopes, S. Laird, D. J. Wilson, P. J. Barnard, C. F. Hogan and P. S. Francis, *Chem. Eur. J.*, 2014, **20**, 3322-3332.
28. S. B. Meier, W. Sarfert, J. M. Junquera-Hernández, M. Delgado, D. Tordera, E. Ortí, H. J. Bolink, F. Kessler, R. Scopelliti, M. Grätzel, M. K. Nazeeruddin and E. Baranoff, *J. Mater. Chem. C*, 2013, **1**, 58-68.
29. J. M. Fernández-Hernández, S. Ladouceur, Y. Shen, A. Iordache, X. Wang, L. Donato, S. Gallagher-Duval, M. d. A. Villa, J. D. Slinker, L. D. Cola and E. Zysman-Colman, *J. Mater. Chem. C*, 2013, **1**, 7440-7452.
30. S. Evariste, M. Sandroni, T. W. Rees, C. Roldán-Carmona, L. Gil-Escrig, H. J. Bolink, E. Baranoff and E. Zysman-Colman, *J. Mater. Chem. C*, 2014, **2**, 5793-5804.
31. T. Hu, L. Duan, J. Qiao, L. He, D. Zhang, R. Wang, L. Wang and Y. Qiu, *Org. Electron.*, 2012, **13**, 1948-1955.
32. S. Ladouceur, D. Fortin and E. Zysman-Colman, *Inorg. Chem.*, 2011, **50**, 11514-11526.
33. C. D. Sunesh, M. Chandran, G. Mathai and Y. Choe, *Optic. Mater.*, 2013, **35**, 407-413.
34. D. Tordera, A. M. Bunzli, A. Pertegas, J. M. Junquera-Hernandez, E. C. Constable, J. A. Zampese, C. E. Housecroft, E. Ortí and H. J. Bolink, *Chem. Eur. J.*, 2013, **19**, 8597-8609.
35. J. Zhang, L. Zhou, H. A. Al-Attar, K. Shao, L. Wang, D. Zhu, Z. Su, M. R. Bryce and A. P. Monkman, *Adv. Funct. Mater.*, 2013, **23**, 4667-4677.
36. F. Kessler, R. D. Costa, D. Di Censo, R. Scopelliti, E. Ortí, H. J. Bolink, S. Meier, W. Sarfert, M. Grätzel, M. K. Nazeeruddin and E. Baranoff, *Dalton Trans.*, 2012, **41**, 180-191.
37. H.-F. Chen, C. Wu, M.-C. Kuo, M. E. Thompson and K.-T. Wong, *J. Mater. Chem.*, 2012, **22**, 9556-9561.
38. E. F. Reid, V. C. Cook, D. J. Wilson and C. F. Hogan, *Chem. Eur. J.*, 2013, **19**, 15907-15917.
39. S. Zanarini, M. Felici, G. Valenti, M. Marcaccio, L. Prodi, S. Bonacchi, P. Contreras-Carballada, R. M. Williams, M. C. Feiters, R. J. Nolte, L. De Cola and F. Paolucci, *Chem. Eur. J.*, 2011, **17**, 4640-4647.
40. G. Valenti, C. Bruno, S. Rapino, A. Fiorani, E. A. Jackson, L. T. Scott, F. Paolucci and M. Marcaccio, *J. Phys. Chem. C*, 2010, **114**, 19467-19472.
41. L. Lin, Y. Wen, Y. Liang, N. Zhang and D. Xiao, *Anal. Methods*, 2013, **5**, 457-464.
42. T. Nobeshima, M. Nakakomi, K. Nakamura and N. Kobayashi, *Adv. Optical Mater.*, 2013, **1**, 144-149.
43. G. Valenti, E. Rampazzo, S. Bonacchi, T. Khajvand, R. Juris, M. Montalti, M. Marcaccio, F. Paolucci and L. Prodi, *Chem. Commun.*, 2012, **48**, 4187-4189.
44. E. H. Doeven, E. M. Zammit, G. J. Barbante, C. F. Hogan, N. W. Barnett and P. S. Francis, *Angew. Chem. Int. Ed.*, 2012, **51**, 4354-4357.
45. E. H. Doeven, E. M. Zammit, G. J. Barbante, P. S. Francis, N. W. Barnett and C. F. Hogan, *Chem. Sci.*, 2013, **4**, 977-982.
46. E. H. Doeven, G. J. Barbante, E. Kerr, C. F. Hogan, J. A. Endler and P. S. Francis, *Anal. Chem.*, 2014, **86**, 2727-2732.
47. L. Yu, Z. Huang, Y. Liu and M. Zhou, *J. Organomet. Chem.*, 2012, **718**, 14-21.
48. B. K. Gorityala, J. Ma, X. Wang, P. Chen and X. W. Liu, *Chem. Soc. Rev.*, 2010, **39**, 2925-2934.
49. Y. Chen, A. Star and S. Vidal, *Chem. Soc. Rev.*, 2013, **42**, 4532-4542.
50. M. J. Li, P. Jiao, M. Lin, W. He, G. N. Chen and X. Chen, *Analyst*, 2011, **136**, 205-210.
51. J. Suk, P. Natarajan, J. N. Moorthy and A. J. Bard, *J. Am. Chem. Soc.*, 2012, **134**, 3451-3460.
52. P. Natarajan and M. Schmittel, *J. Org. Chem.*, 2012, **77**, 8669-8677.
53. J. Suk, Z. Wu, L. Wang and A. J. Bard, *J. Am. Chem. Soc.*, 2011, **133**, 14675-14685.
54. H. Qi, J. Chang, S. H. Abdelwahed, K. Thakur, R. Rathore and A. J. Bard, *J. Am. Chem. Soc.*, 2012, **134**, 16265-16274.
55. H.-F. Chen, C.-T. Liao, T.-C. Chen, H.-C. Su, K.-T. Wong and T.-F. Guo, *J. Mater. Chem.*, 2011, **21**, 4175-4181.
56. H.-F. Chen, C.-T. Liao, M.-C. Kuo, Y.-S. Yeh, H.-C. Su and K.-T. Wong, *Org. Electron.*, 2012, **13**, 1765-1773.
57. K. N. Swanick, J. T. Price, N. D. Jones and Z. Ding, *J. Org. Chem.*, 2012, **77**, 5646-5655.
58. M. M. Richter, *Chem. Rev.*, 2004, **104**, 3003-3036.
59. X. Liu, W. Qi, W. Gao, Z. Liu, W. Zhang, Y. Gao and G. Xu, *Chem. Commun.*, 2014, **50**, 14662-14665.
60. R. Ishimatsu, S. Matsunami, T. Kasahara, J. Mizuno, T. Edura, C. Adachi, K. Nakano and T. Imato, *Angew. Chem. Int. Ed.*, 2014, **53**, 6993-6996.
61. M. Shen, X. H. Zhu and A. J. Bard, *J. Am. Chem. Soc.*, 2013, **135**, 8868-8873.
62. F. Polo, F. Rizzo, M. Veiga-Gutierrez, L. De Cola and S. Quici, *J. Am. Chem. Soc.*, 2012, **134**, 15402-15409.
63. M. Amelia, C. Lincheneau, S. Silvi and A. Credi, *Chem. Soc. Rev.*, 2012, **41**, 5728-5743.
64. P. Wu, X. Hou, J. J. Xu and H. Y. Chen, *Chem. Rev.*, 2014, **114**, 11027-11059.
65. L. Li, H. Liu, Y. Shen, J. Zhang and J. J. Zhu, *Anal. Chem.*, 2011, **83**, 661-665.
66. Y. M. Fang, J. Song, J. Li, Y. W. Wang, H. H. Yang, J. J. Sun and G. N. Chen, *Chem. Commun.*, 2011, **47**, 2369-2371.
67. L. Wu, J. Wang, J. Ren, W. Li and X. Qu, *Chem. Commun.*, 2013, **49**, 5675-5677.
68. Y. Xu, M. Wu, X. Z. Feng, X. B. Yin, X. W. He and Y. K. Zhang, *Chem. Eur. J.*, 2013, **19**, 6282-6288.
69. J. Lu, M. Yan, L. Ge, S. Ge, S. Wang, J. Yan and J. Yu, *Biosens. Bioelectron.*, 2013, **47**, 271-277.
70. Z. Ren, Y. Wei, J. Xiang, S. Zhang, J. Song, C. Mao, H. Niu, B. Jin, J. Wu and Y. Tian, *Anal. Lett.*, 2013, **46**, 1394-1403.
71. L.-L. Li, J. Ji, R. Fei, C.-Z. Wang, Q. Lu, J.-R. Zhang, L.-P. Jiang and J.-J. Zhu, *Adv. Funct. Mater.*, 2012, **22**, 2971-2979.
72. C. Cheng, Y. Huang, X. Tian, B. Zheng, Y. Li, H. Yuan, D. Xiao, S. Xie and M. M. Choi, *Anal. Chem.*, 2012, **84**, 4754-4759.
73. C. Cheng, Y. Huang, J. Wang, B. Zheng, H. Yuan and D. Xiao, *Anal. Chem.*, 2013, **85**, 2601-2605.
74. L. Chen, D. Huang, S. Ren, T. Dong, Y. Chi and G. Chen, *Nanoscale*, 2013, **5**, 225-230.
75. L. Chen, X. Zeng, P. Si, Y. Chen, Y. Chi, D. H. Kim and G. Chen, *Anal. Chem.*, 2014, **86**, 4188-4195.

76. K. N. Swanick, M. Hesari, M. S. Workentin and Z. Ding, *J. Am. Chem. Soc.*, 2012, **134**, 15205-15208.
77. M. Hesari, M. S. Workentin and Z. Ding, *Chem. Sci.*, 2014, **5**, 3814-3822.
78. M. Hesari, M. S. Workentin and Z. Ding, *ACS Nano*, 2014, **8**, 8543-8553.
79. W. Guo, J. Yuan and E. Wang, *Chem. Commun.*, 2012, **48**, 3076-3078.
80. L. Luan, Z. J. Lin, G. Wu, X. L. Huang, Z. M. Cai and X. Chen, *Chem. Commun.*, 2011, **47**, 3963-3965.
81. F. Pinaud, L. Russo, S. Pinet, I. Gosse, V. Ravaine and N. Sojic, *J. Am. Chem. Soc.*, 2013, **135**, 5517-5520.
82. W. Wang, T. Xiong and H. Cui, *Langmuir*, 2008, **24**, 2826-2833.
83. D. Tian, H. Zhang, Y. Chai and H. Cui, *Chem. Commun.*, 2011, **47**, 4959-4961.
84. Y. Chai, D. Tian, J. Gu and H. Cui, *Analyst*, 2011, **136**, 3244-3251.
85. Y. Zhou, Y. Zhuo, N. Liao, Y. Chai and R. Yuan, *Chem. Commun.*, 2014, **50**, 14627-14630.
86. H. F. Zhao, R. P. Liang, J. W. Wang and J. D. Qiu, *Biosens. Bioelectron.*, 2015, **63**, 458-464.
87. F. Li, Y. Yu, H. Cui, D. Yang and Z. Bian, *Analyst*, 2013, **138**, 1844-1850.
88. F. Li and H. Cui, *Biosens. Bioelectron.*, 2013, **39**, 261-267.
89. X. Yu and H. Cui, *Electrochim. Acta*, 2014, **125**, 156-162.
90. L. Zhang, W. Niu, Z. Li and G. Xu, *Chem. Commun.*, 2011, **47**, 10353-10355.
91. L. Zhang, W. Niu, W. Gao, S. Majeed, Z. Liu, J. Zhao, S. Anjum and G. Xu, *Chem. Commun.*, 2013, **49**, 8836-8838.
92. L. Zhang, W. Niu, J. Zhao, S. Zhu, Y. Yuan, T. Yuan, L. Hu and G. Xu, *Faraday Discuss.*, 2013, **164**.
93. L. Zhang, W. Niu, W. Gao, L. Qi, J. Lai, J. Zhao and G. Xu, *ACS Nano*, 2014, **8**, 5953-5958.
94. Q. Li, C. Zhang, J. Y. Zheng, Y. S. Zhao and J. Yao, *Chem. Commun.*, 2012, **48**, 85-87.
95. M. Yin, L. Wu, Z. Li, J. Ren and X. Qu, *Nanoscale*, 2012, **4**, 400-404.
96. L. Wu, J. Wang, M. Yin, J. Ren, D. Miyoshi, N. Sugimoto and X. Qu, *Small*, 2014, **10**, 330-336.
97. T. Hu, X. Liu, S. Liu, Z. Wang and Z. Tang, *Anal. Chem.*, 2014, **86**, 3939-3946.
98. W. Qi, D. Wu, J. Zhao, Z. Liu, W. Zhang, L. Zhang and G. Xu, *Anal. Chem.*, 2013, **85**, 3207-3212.
99. W. Qi, M. Xu, L. Pang, Z. Liu, W. Zhang, S. Majeed and G. Xu, *Chem. Eur. J.*, 2014, **20**, 4829-4835.
100. J. L. Adcock, P. S. Francis and N. W. Barnett, *Anal. Chim. Acta*, 2007, **601**, 36-67.
101. R. Kurita, K. Arai, K. Nakamoto, D. Kato and O. Niwa, *Anal. Chem.*, 2010, **82**, 1692-1697.
102. R. Kurita, K. Arai, K. Nakamoto, D. Kato and O. Niwa, *Anal. Chem.*, 2012, **84**, 1799-1803.
103. N. P. Sardesai, J. C. Barron and J. F. Rusling, *Anal. Chem.*, 2011, **83**, 6698-6703.
104. Y. Zhuo, N. Liao, Y. Q. Chai, G. F. Gui, M. Zhao, J. Han, Y. Xiang and R. Yuan, *Anal. Chem.*, 2014, **86**, 1053-1060.
105. Y. Zhang, W. Liu, S. Ge, M. Yan, S. Wang, J. Yu, N. Li and X. Song, *Biosens. Bioelectron.*, 2013, **41**, 684-690.
106. X. Zhang, J. Li, C. Chen, B. Lou, L. Zhang and E. Wang, *Chem. Commun.*, 2013, **49**, 3866-3868.
107. S. Wang, W. Dai, L. Ge, M. Yan, J. Yu, X. Song, S. Ge and J. Huang, *Chem. Commun.*, 2012, **48**, 9971-9973.
108. W. Li, L. Li, S. Ge, X. Song, L. Ge, M. Yan and J. Yu, *Chem. Commun.*, 2013, **49**, 7687-7689.
109. Y. Zhang, L. Ge, M. Li, M. Yan, S. Ge, J. Yu, X. Song and B. Cao, *Chem. Commun.*, 2014, **50**, 1417-1419.
110. J. Wang, H. Han, X. Jiang, L. Huang, L. Chen and N. Li, *Anal. Chem.*, 2012, **84**, 4893-4899.
111. G. Liang, S. Liu, G. Zou and X. Zhang, *Anal. Chem.*, 2012, **84**, 10645-10649.
112. K. Shao, J. Wang, X. Jiang, F. Shao, T. Li, S. Ye, L. Chen and H. Han, *Anal. Chem.*, 2014, **86**, 5749-5757.
113. S. Xu, Y. Liu, T. Wang and J. Li, *Anal. Chem.*, 2010, **82**, 9566-9572.
114. S. Xu, Y. Liu, T. Wang and J. Li, *Anal. Chem.*, 2011, **83**, 3817-3823.
115. H. Niu, R. Yuan, Y. Chai, L. Mao, Y. Yuan, Y. Cao and Y. Zhuo, *Chem. Commun.*, 2011, **47**, 8397-8399.
116. Y. Cheng, R. Yuan, Y. Chai, H. Niu, Y. Cao, H. Liu, L. Bai and Y. Yuan, *Anal. Chim. Acta*, 2012, **745**, 137-142.
117. H. Niu, R. Yuan, Y. Chai, L. Mao, Y. Yuan, Y. Zhuo, S. Yuan and X. Yang, *Biosens. Bioelectron.*, 2011, **26**, 3175-3180.
118. H. Wang, R. Yuan, Y. Chai, H. Niu, Y. Cao and H. Liu, *Biosens. Bioelectron.*, 2012, **37**, 6-10.
119. Y. Chen, J. Xu, J. Su, Y. Xiang, R. Yuan and Y. Chai, *Anal. Chem.*, 2012, **84**, 7750-7755.
120. Y. Li, X. Luo, Z. Yan, J. Zheng and H. Qi, *Chem. Commun.*, 2013, **49**, 3869-3871.
121. R. Duan, X. Zhou and D. Xing, *Anal. Chem.*, 2010, **82**, 3099-3103.
122. C. Li, J. Lin, Y. Guo and S. Zhang, *Chem. Commun.*, 2011, **47**, 4442-4444.
123. Y. Chai, D. Tian, W. Wang and H. Cui, *Chem. Commun.*, 2010, **46**, 7560-7562.
124. F. Li, Y. Yu, Q. Li, M. Zhou and H. Cui, *Anal. Chem.*, 2014, **86**, 1608-1613.
125. X. Tang, D. Zhao, J. He, F. Li, J. Peng and M. Zhang, *Anal. Chem.*, 2013, **85**, 1711-1718.
126. X. Zhou, D. Zhu, Y. Liao, W. Liu, H. Liu, Z. Ma and D. Xing, *Nat. Protoc.*, 2014, **9**, 1146-1159.
127. F. Divsar and H. Ju, *Chem. Commun.*, 2011, **47**, 9879-9881.
128. Y. Chen, B. Jiang, Y. Xiang, Y. Chai and R. Yuan, *Chem. Commun.*, 2011, **47**, 7758-7760.
129. L. Chen, Q. Cai, F. Luo, X. Chen, X. Zhu, B. Qiu, Z. Lin and G. Chen, *Chem. Commun.*, 2010, **46**, 7751-7753.
130. J. Dang, Z. Guo and X. Zheng, *Anal. Chem.*, 2014, **86**, 8943-8950.
131. Z. Liu, W. Zhang, L. Hu, H. Li, S. Zhu and G. Xu, *Chem. Eur. J.*, 2010, **16**, 13356-13359.
132. T. Yuan, Z. Liu, L. Hu, L. Zhang and G. Xu, *Chem. Commun.*, 2011, **47**, 11951-11953.
133. J. Yan, M. Yan, L. Ge, J. Yu, S. Ge and J. Huang, *Chem. Commun.*, 2013, **49**, 1383-1385.
134. G. Jie, L. Wang, J. Yuan and S. Zhang, *Anal. Chem.*, 2011, **83**, 3873-3880.
135. C. Ding, S. Wei and H. Liu, *Chem. Eur. J.*, 2012, **18**, 7263-7268.
136. M. S. Wu, D. J. Yuan, J. J. Xu and H. Y. Chen, *Anal. Chem.*, 2013, **85**, 11960-11965.
137. C. X. Tang, N. N. Bu, X. W. He and X. B. Yin, *Chem. Commun.*, 2011, **47**, 12304-12306.
138. A. Gao, C. X. Tang, X. W. He and X. B. Yin, *Analyst*, 2013, **138**, 263-268.
139. H. Zhou, Y. Y. Zhang, J. Liu, J. J. Xu and H. Y. Chen, *Chem. Commun.*, 2013, **49**, 2246-2248.
140. L. Hou, Z. Gao, M. Xu, X. Cao, X. Wu, G. Chen and D. Tang, *Biosens. Bioelectron.*, 2014, **54**, 365-371.
141. Y. Liao, R. Yuan, Y. Chai, Y. Zhuo, Y. Yuan, L. Bai, L. Mao and S. Yuan, *Biosens. Bioelectron.*, 2011, **26**, 4815-4818.
142. M. Zhang, S. Ge, W. Li, M. Yan, X. Song, J. Yu, W. Xu and J. Huang, *Analyst*, 2012, **137**, 680-685.
143. J. Ballesta-Claver, R. Rodriguez-Gomez and L. F. Capitán-Vallvey, *Anal. Chim. Acta*, 2013, **770**, 153-160.
144. W. Gao, Y. Chen, J. Xi, S. Lin, Y. Lin and Z. Chen, *Biosens. Bioelectron.*, 2013, **41**, 776-782.
145. Y. Xu, Z. Lv, Y. Xia, Y. Han, B. Lou and E. Wang, *Anal. Bioanal. Chem.*, 2013, **405**, 3549-3558.
146. D. Shan, B. Qian, S.-N. Ding, W. Zhu, S. Cosnier and H.-G. Xue, *Anal. Chem.*, 2010, **82**, 5892-5896.
147. Q. Li, J. Y. Zheng, Y. Yan, Y. S. Zhao and J. Yao, *Adv. Mater.*, 2012, **24**, 4745-4749.
148. Y. Yuan, H. Li, S. Han, L. Hu, S. Parveen, H. Cai and G. Xu, *Anal. Chim. Acta*, 2012, **720**, 38-42.
149. A. Arora, J. C. T. Eijkel, W. E. Morf and A. Manz, *Anal. Chem.*, 2001, **73**, 3282-3288.
150. X. Lin, L. Zheng, G. Gao, Y. Chi and G. Chen, *Anal. Chem.*, 2012, **84**, 7700-7707.
151. M. S. Wu, B. Y. Xu, H. W. Shi, J. J. Xu and H. Y. Chen, *Lab on a chip*, 2011, **11**, 2720-2724.
152. B. Y. Chang, K. F. Chow, J. A. Crooks, F. Mavre and R. M. Crooks, *Analyst*, 2012, **137**, 2827-2833.

153. M. S. Wu, G. S. Qian, J. J. Xu and H. Y. Chen, *Anal. Chem.*, 2012, **84**, 5407-5414.
154. M.-S. Wu, D.-J. Yuan, J.-J. Xu and H.-Y. Chen, *Chem. Sci.*, 2013, **4**, 1182-1188.
- 5 155. X. Zhang, C. Chen, J. Li, L. Zhang and E. Wang, *Anal. Chem.*, 2013, **85**, 5335-5339.
156. L. Ge, S. Wang, S. Ge, J. Yu, M. Yan, N. Li and J. Huang, *Chem. Commun.*, 2014, **50**, 5699-5702.
157. M. Sentic, G. Loget, D. Manojlovic, A. Kuhn and N. Sojic, *Angew. Chem. Int. Ed.*, 2012, **51**, 11284-11288.
- 10 158. M. Sentic, S. Arbault, B. Goudeau, D. Manojlovic, A. Kuhn, L. Bouffier and N. Sojic, *Chem. Commun.*, 2014, **50**, 10202-10205.
159. W. Qi, J. Lai, W. Gao, S. Li, S. Hanif and G. Xu, *Anal. Chem.*, 2014, **86**, 8927-8931.
- 15 160. J. Rodriguez-Lopez, M. Shen, A. B. Nepomnyashchii and A. J. Bard, *J. Am. Chem. Soc.*, 2012, **134**, 9240-9250.
161. J. S. Yuk, E. O'Reilly, R. J. Forster, B. D. MacCraith and C. McDonagh, *Chem. Phys. Lett.*, 2011, **513**, 112-117.
162. D. Wang, L. Guo, R. Huang, B. Qiu, Z. Lin and G. Chen, *Electrochim. Acta*, 2014, **150**, 123-128.
- 20 163. D. Wang, L. Guo, R. Huang, B. Qiu, Z. Lin and G. Chen, *Sci. Rep.*, 2015, **5**, 7954.
164. G. A. Crespo, G. Mistlberger and E. Bakker, *J. Am. Chem. Soc.*, 2012, **134**, 205-207.
- 25 165. O. V. Klymenko, I. Svir and C. Amatore, *Chemphyschem : a European journal of chemical physics and physical chemistry*, 2013, **14**, 2237-2250.
166. J. B. Ketter, S. P. Forry, R. M. Wightman and S. W. Feldberg, *Electrochem. Solid-State Lett.*, 2004, **7**, E18-E22.
- 30 167. M. M. Sartin, C. Shu and A. J. Bard, *J. Am. Chem. Soc.*, 2008, **130**, 5354-5360.
168. C. Amatore, O. Klymenko and I. Svir, *Electrochem. Commun.*, 2010, **12**, 1170-1173.
169. C. Amatore, O. Klymenko and I. Svir, *Electrochem. Commun.*, 35 2010, **12**, 1165-1169.
170. O. V. Klymenko, I. Svir, A. I. Oleinick and C. Amatore, *Chemphyschem : a European journal of chemical physics and physical chemistry*, 2012, **13**, 845-859.
171. C. Amatore, O. V. Klymenko and I. Svir, *Anal. Chem.*, 2012, 40 **84**, 2792-2798.
172. I. Svir, A. Oleinick, O. V. Klymenko and C. Amatore, *ChemElectroChem*, 2015, DOI: 10.1002/celec.201402460.
173. S. v. Reenen, P. Matyba, A. Dzwilewski, R. A. J. Janssen, L. Edman and M. Kemerink, *Adv. Funct. Mater.*, 2011, **21**, 1795-1802.
- 45 174. T. Daimon and E. Nihei, *J. Mater. Chem. C*, 2013, **1**, 2826-2833.
175. S. Tang, J. Pan, H. A. Buchholz and L. Edman, *J. Am. Chem. Soc.*, 2013, **135**, 3647-3652.
176. C.-S. Tsai, S.-H. Yang, B.-C. Liu and H.-C. Su, *Org. Electron.*, 50 2013, **14**, 488-499.
177. X. Y. Zeng, Q. K. Zhang, R. M. Yu and C. Z. Lu, *Adv. Mater.*, 2010, **22**, 4484-4488.
178. Z. Yu, X. Niu, Z. Liu and Q. Pei, *Adv. Mater.*, 2011, **23**, 3989-3994.
- 55 179. P. Matyba, H. Yamaguchi, M. Chhowalla, N. D. Robinson and L. Edman, *ACS Nano*, 2011, **5**, 574-580.
180. J. Liu, I. Engquist, X. Crispin and M. Berggren, *J. Am. Chem. Soc.*, 2012, **134**, 901-904.
181. J. Liu, I. Engquist and M. Berggren, *J. Am. Chem. Soc.*, 2013, 60 **135**, 12224-12227.
182. R. D. Costa, E. Orti, H. J. Bolink, F. Monti, G. Accorsi and N. Armaroli, *Angew. Chem. Int. Ed.*, 2012, **51**, 8178-8211.
183. M. Mydlak, C. Bizzarri, D. Hartmann, W. Sarfert, G. Schmid and L. De Cola, *Adv. Funct. Mater.*, 2010, **20**, 1812-1820.
- 65 184. H. C. Moon, T. P. Lodge and C. D. Frisbie, *J. Am. Chem. Soc.*, 2014, **136**, 3705-3712.
185. H.-C. Su, H.-F. Chen, P.-H. Chen, S.-W. Lin, C.-T. Liao and K.-T. Wong, *J. Mater. Chem.*, 2012, **22**, 22998-23004.
186. H.-B. Wu, H.-F. Chen, C.-T. Liao, H.-C. Su and K.-T. Wong, 70 *Org. Electron.*, 2012, **13**, 483-490.
187. H.-C. Su, H.-F. Chen, Y.-C. Shen, C.-T. Liao and K.-T. Wong, *J. Mater. Chem.*, 2011, **21**, 9653-9660.
188. T. Akatsuka, C. Roldan-Carmona, E. Orti and H. J. Bolink, *Adv. Mater.*, 2014, **26**, 770-774.
- 75 189. R. D. Costa, E. Orti, H. J. Bolink, S. Graber, C. E. Housecroft and E. C. Constable, *Adv. Funct. Mater.*, 2010, **20**, 1511-1520.
190. C.-L. Lee, C.-Y. Cheng and H.-C. Su, *Org. Electron.*, 2014, **15**, 711-720.
191. C. C. Ho, H. F. Chen, Y. C. Ho, C. T. Liao, H. C. Su and K. T. Wong, *Phys. Chem. Chem. Phys.*, 2011, **13**, 17729-17736.
- 80 192. R. D. Costa, E. Orti, H. J. Bolink, S. Graber, C. E. Housecroft and E. C. Constable, *J. Am. Chem. Soc.*, 2010, **132**, 5978-5980.
193. H. J. Bolink, E. Coronado, R. D. Costa, E. Orti, M. Sessolo, S. Graber, K. Doyle, M. Neuberger, C. E. Housecroft and E. C. Constable, *Adv. Mater.*, 2008, **20**, 3910-3913.
- 85 194. S. Graber, K. Doyle, M. Neuberger, C. E. Housecroft, E. C. Constable, R. D. Costa, E. Orti, D. Repetto and H. J. Bolink, *J. Am. Chem. Soc.*, 2008, **130**, 14944 - 14945.
195. R. D. Costa, E. Orti, H. J. Bolink, S. Graber, C. E. Housecroft, 90 M. Neuberger, S. Schaffner and E. C. Constable, *Chem. Commun.*, 2009, **45**, 2029 - 2031.
196. L. He, L. Duan, J. Qiao, D. Zhang, L. Wang and Y. Qiu, *Chem. Commun.*, 2011, **47**, 6467-6469.
197. R. D. Costa, E. Orti, H. J. Bolink, S. Graber, C. E. Housecroft and E. C. Constable, *Chem. Commun.*, 2011, **47**, 3207-3209.
- 95 198. R. D. Costa, E. Orti, D. Tordera, A. Pertegás, H. J. Bolink, S. Graber, C. E. Housecroft, L. Sachno, M. Neuberger and E. C. Constable, *Adv. Energy Mater.*, 2011, **1**, 282-290.
- 100



Zhongyuan Liu obtained her both BSc and MSc in chemistry from Southwest University. She joined Changchun Institute of Applied Chemistry as an assistant professor in 2009. Her research interests focus on electrochemiluminescence, electrochemistry, aptasensors and immunosensors.



Wenjing Qi obtained her both BSc and MSc in chemistry from Southwest University. She received PhD under the guidance of Professor Guobao Xu at University of the Chinese Academy of Sciences. She currently is working at College of chemistry, Chongqing normal university. Her research interests include electrochemiluminescence,

fluorescence, dark-field scattering spectroscopic microscopy with nanospheres.



5 **Guobao Xu** received BSc from
Jilin University, MSc from Xiamen University, and PhD from
Changchun Institute of Chemistry. After postdoctoral research at
University of Hong Kong, Hong Kong Polytechnic University,
and JST-NTT, he joined the Institute in 2004 and currently is
10 FRSC, CChem, and CSci. His research interests include
electrochemiluminescence, nanomaterials, and biosensors. He has
won Young Scholar Award of Chinese Chemical society, Second
Class Award of National Natural Science of China, Excellent
Principal Investigator of One Hundred Talents Program of CAS,
15 Excellent Youth Award of Chinese Society of Electrochemistry,
and SCOPUS Young Researcher Gold Award in Materials
Science.

Cite this: DOI: 10.1039/c0xx00000x

www.rsc.org/xxxxxx

ARTICLE TYPE

Recent advances in electrochemiluminescence

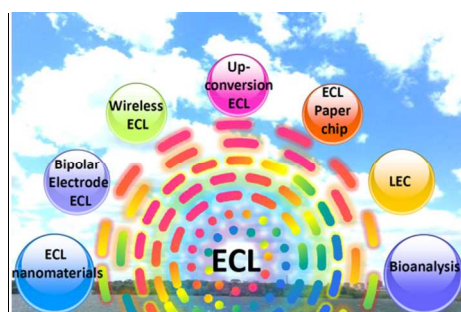
Zhongyuan Liu†^a, Wenjing Qi†^{a,b} and Guobao Xu*^a

Received (in XXX, XXX) Xth XXXXXXXXX 20XX, Accepted Xth XXXXXXXXX 20XX

First published on the web Xth XXXXXXXXX 20XX

DOI: 10.1039/b000000x

Graphical content entry:



Recent advances, novel phenomena, and prospectives in electrochemiluminescence are presented.

10